Brightly Luminescent Platinum Complexes of *N^C^-^N* Ligands Forming Six-Membered Chelate Rings: Offsetting Deleterious Ring Size Effects Using Site-Selective Benzannulation

Robert J. Ortiz,[a] Jason D. Braun,[a] J. A. Gareth Williams[b] and David E. Herbert[a]**

[a] Department of Chemistry and the Manitoba Institute for Materials, University of Manitoba, 144 Dysart Road, Winnipeg, Manitoba, R3T 2N2, Canada

*david.herbert@umanitoba.ca

[b] Department of Chemistry, Durham University, Durham, DH1 3LE, UK

*j.a.g.williams@durham.ac.uk

ABSTRACT

Brightly emissive platinum(II) complexes ($\lambda_{emission,\ max}$ = 607-612 nm) of the type ^{R}**L**PtCl are reported, where ^{R}**L** is a cyclometallated *N^C–^N*-coordinating ligand derived from 1,3-di(2-trifluoromethyl-4-phenanthridinyl)benzene (^{CF3}**LH**) or 1,3-di(2-*tert*-butyl-4-phenanthridinyl)benzene ($^{t\mathrm{Bu}}$**LH**). Metathesis of the chlorido ligand can be achieved under mild conditions, enabling isolation of ionic compounds with the formula [^{CF3}**L**PtL']PF_6 where L' = pyridine or (4-dimethylamino)pyridine (DMAP), as well as the charge-neutral species $^{t\mathrm{Bu}}$**L**Pt(C≡C-C_6H_4-*t*Bu) (C≡C-C_6H_4-*t*Bu = 4-*tert*-butylphenylacetylido). Compared with *N^N^N*-ligated Pt(II) complexes that form 5-membered chelates, these compounds all contain 6-membered rings. Expanding chelate ring size from 5 to 6 has been previously demonstrated to enhance emission in some *N^N^N*-coordinated Pt(II) species – for example, in complexes of 2,6-di(8-quinolinyl)pyridine vs. those of 2,2':6',2''-terpyridine – but in related *N^C–^N*-coordinated species, luminescence quantum yields are significantly lower for the 6-membered chelate ring complexes. Here, we demonstrate that site-selective benzannulation of the quinolinyl side-arms can offset the deleterious effect of changing the chelate ring-size and boost photophysical properties such as the quantum yield. Density functional theory (DFT) and time-dependent DFT (TDDFT) calculations suggest that benzannulation counterintuitively destabilizes the emissive triplet states compared to the smaller π-system, with the 'imine-bridged biphenyl' form of the phenanthridinyl arm helping to buffer against larger molecular distortions, enhancing photoluminescence quantum yields up to 0.09 ± 0.02. The spontaneous formation under aerated conditions of a Pt(IV) derivative ^{CF3}**L**$PtCl_3$ is also reported, together with its molecular structure in the solid state.

INTRODUCTION

Phosphorescent chromophores are in continual demand for applications ranging from chemosensing[1,2] to bioimaging[3–5], light emitting diodes[6–8] and artificial photosynthesis.[9] Square-planar platinum(II) complexes are particularly useful in such contexts thanks to the strong spin-orbit coupling (SOC) of the heavy element[10] combined with a developed understanding of how ligand design[11] can be used to destabilize deactivating metal-centered (MC) states in favor of luminescent charge-transfer (CT) ones. Cyclometallated ligands based on aryl-substituted heterocycles exert strong ligand fields through the synergy of σ donation and π acceptance and so are particularly useful, evidenced, for example, by the contrast between $[Pt(tpy)Cl]^+$ (tpy = 2,2':6',2''-terpyridine), which is barely emissive at room temperature (Φ_{lum} = 0.0004),[12] and Pt(dpyb)Cl which is brightly phosphorescent (dpybH = 1,3-di(2-pyridyl)benzene; τ = 7.2 μs, Φ_{lum} = 0.6; Figure 1).[13]

Beyond altering donicity, changing a chelating ligand's bite angle can also boost quantum yields by improving orbital overlap. For example, tridentate *N^N^N* scaffolds that form six-membered rings may display more intense emission than analogs with five-membered rings, as in the case of $[Pt(dqpy)Cl]PF_6$ (τ = 16 μs, Φ_{lum} = 0.036 in dichloromethane at room temperature; dqpy = 1,3-di(8-quinolyl)pyridine),[14] again compared with $[Pt(tpy)Cl]^+$. In that case, exchange of 2-substituted pyridines for 8-substituted quinolines relaxes the constraints placed on the ligand in adopting the preferred square-planar geometry of Pt(II): a nearly linear N-Pt-N bond angle of 178.8° is observed, contrasting a much more acute 163.5° in $[Pt(tpy)Cl]ClO_4$.[15] This also strengthens the ligand field, destabilizing metal-centred excited states, favoring emission. A similar trend is well-documented for pseudo-octahedral Ru(II) complexes containing tridentate ligands.[16,17] Yet, for cyclometallated *N^C⁻^N*-coordinated Pt(II) emitters, increasing chelate ring size to improve the bite angle proved to have the opposite effect: compared with Pt(dpyb)Cl which boasts five-membered chelate rings, Pt(dqb)Cl (dqb = 1,3-di(8-quinolyl)benzene) exhibits a significantly lower radiative rate constant (k_r = 1100 versus 83000 s^{-1}; attributed to diminished metal participation in the excited state) and hence a much smaller quantum yield

(0.016).[14] Similarly, a tridentate ligand that binds via 6-membered chelate rings using 7-*N*-substituted azaindole moieties was found to be non-emissive,[14] as was the *N*^*C*^*N*-coordinated Pt(II) complex of 1,8-bis(2-pyridyl)anthracene[18] despite an ostensibly more favorable ligand geometry at the metal center in both cases.

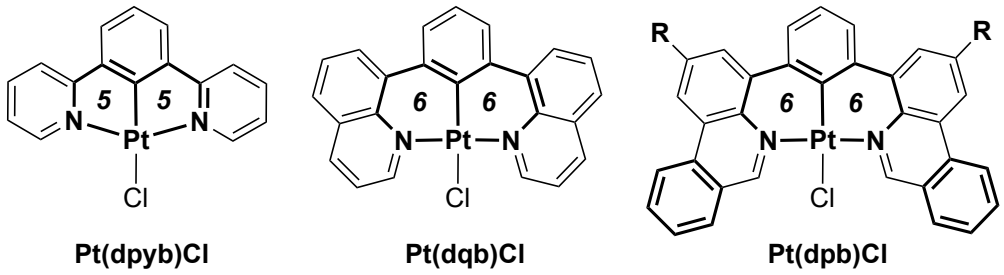

Figure 1. Structures of Pt(dpyb)Cl[13], Pt(dqb)Cl[14] and Pt(dpb)Cl (dpb = 1,3-di(4-phenathridinyl)benzene; this work) with the respective chelate ring sizes indicated in italics.

We recently demonstrated that introducing site-selective benzannulation in the form of phenanthridinyl (3,4-benzoquinoline) units to chelating, pincer-like diarylamido scaffolds can boost the phosphorescence intensity from their Pt(II) complexes. These emit in the deep red, with unusually narrow emission band shapes. Despite prevailing expectations, site-selective benzannulation induces a significant shift of emission to higher energy, decreasing the observed Stokes' shift through heightened molecular rigidity owed to the phenanthridinyl units enhanced ability to resist molecular reorganization in their excited states compared to quinolinyl congeners.[19] Substituents in the 2-position of the phenanthridinyl arms can further modulate luminescence, contingent on the substituent's electron donor/acceptor character.[20] Curious as to the ability of ligand benzannulation to potentially offset the deleterious effect of increased chelate-ring size in cyclometallated Pt(II) emitters by impacting radiative/non-radiative decay rates, we decided to investigate the use of site-selective benzannulation to construct cyclometallated pincer-type ligands that combine a central aryl donor with flanking, 6-membered chelate-forming, phenanthridinyl arms. Platinum chlorido complexes of these ligands are

impressively bright emitters, indicating that 6-membered chelates are not necessarily detrimental to the photophysical properties of tridentate cyclometallated platinum complexes.

RESULTS AND DISCUSSION

Ligand and Complex Design and Synthesis

The ligands and complexes reported in this study are summarized in Scheme 1. Two phenanthridinyl *N^C*(H)^*N* proligands, containing either an electron-withdrawing trifluoromethyl group (**^{CF3}LH**) or an electron-releasing *tert*-butyl substituent (**^{tBu}LH**) in the 2-position of the phenanthridinyl moieties, were prepared via Pd-catalyzed cross-coupling of the respective 4-bromophenanthridines with benzene-1,3-diboronic acid (Scheme 1a). The identity of the substituent on the phenanthridine ring did not significantly influence the isolated yield of the proligand (**^{CF3}LH**: 76%, **^{tBu}LH**: 68%), but their different solubilities did dictate how they were isolated (see Experimental Section and SI for details).

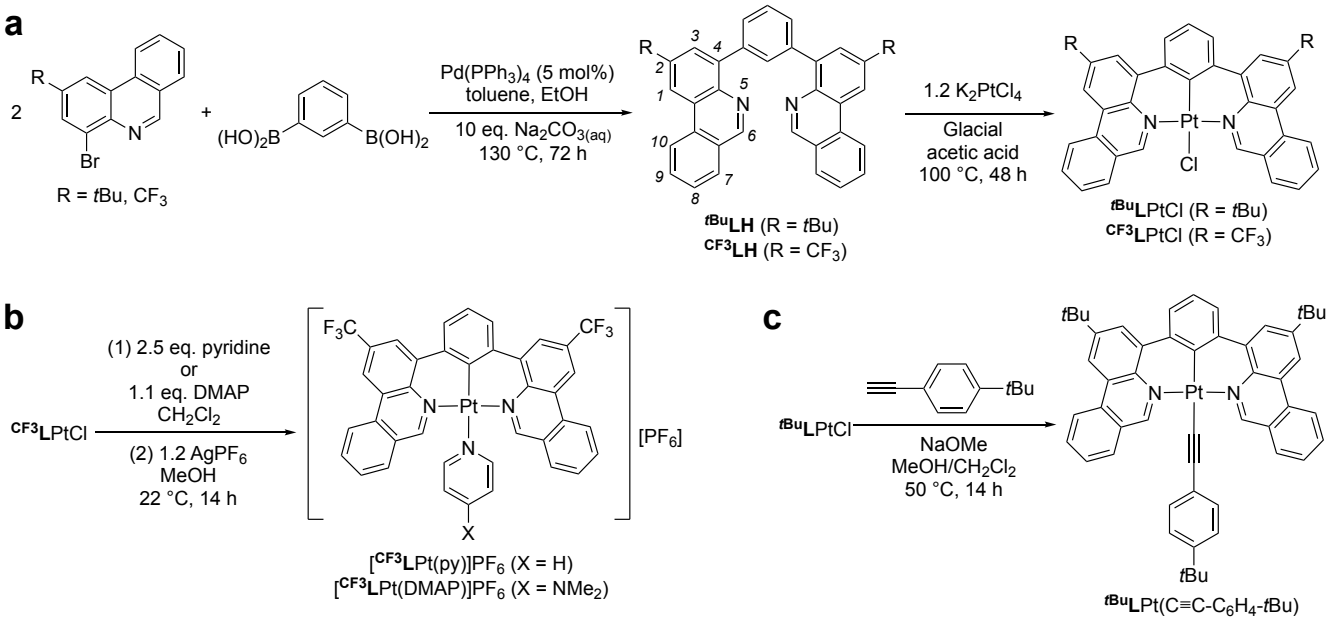

Scheme 1. Synthesis of (a) proligands **^{R}LH** (R = CF_3, *t*Bu) and their platinum(II) chlorido complexes **^{R}L**PtCl (R = CF_3, *t*Bu), (b) ionic analogs [**^{CF3}L**PtL']PF_6 (L' = pyridine, DMAP) and (c) the acetylido derivative **^{tBu}L**Pt(C≡C-C_6H_4-*t*Bu). The IUPAC numbering system for phenanthridines is illustrated for **^{R}LH**.

Complexation of the proligands to platinum was then pursued[21] by heating a mixture of the corresponding proligand and potassium tetrachloridoplatinate in glacial acetic acid to 100 °C under an argon atmosphere (Scheme 1a). Both ^{CF3}**L**PtCl and ^{tBu}**L**PtCl precipitated from the reaction mixture and were isolated by vacuum filtration as yellow powders in 85 and 79% yield, respectively. As with the proligands, the solubility of ^{tBu}**L**PtCl was superior to ^{CF3}**L**PtCl, which were both characterized in solution via multinuclear NMR. ^{1}H NMR spectroscopy confirmed the coordination of the ligand to platinum through three distinct features, as highlighted for ^{tBu}**L**PtCl: (1) the disappearance of the central aryl proton resonance ($C_{16}H$; triplet at 8.11 ppm in ^{tBu}**LH**); (2) a downfield shift of the phenanthridinyl *H*C=N resonances (9.34 ppm in ^{tBu}**LH** to 10.17 ppm); and (3), the appearance of ^{195}Pt satellites for this signal ($^{3}J_{PtH}$ = 46.2 Hz). The downfield shift of the *H*C=N proton resonance upon binding to an electrophilic transition metal center is a consistent feature of square-planar Group 10 coordination complexes of phenanthridinyl-based pincer-type ligand frameworks.[22,23]

Interestingly, while the complexes were judged to be generally stable to ambient air and moisture, diffusion of hexanes vapor into a chloroform solution of ^{CF3}**L**PtCl over 3 months[24] deposited crystals of an oxidized trichlorido Pt(IV) species (^{CF3}**L**PtCl$_3$) indicating that ^{CF3}**L**PtCl is unstable towards oxidation via reaction with chloroform over longer time periods. Indeed, refluxing ^{CF3}**LH** with K_2PtCl_4 in glacial acetic acid under an aerobic atmosphere led to the appearance of a new resonance in the ^{19}F NMR spectrum (δ -62.0 ppm) just downfield of the peak assigned to ^{CF3}**L**PtCl. Further reflux of this mixture as a chloroform suspension led to a maximum of 93% conversion to ^{CF3}**L**PtCl$_3$ by ^{19}F NMR, with a persistent 7% ^{CF3}**L**PtCl remaining. The increased solubility of the Pt(IV) species enabled assignment of its ^{1}H NMR spectrum, which shows evidence of binding with a smaller Pt-H coupling constant ($^{3}J_{PtH}$ = 33.5 Hz) of the C*H*=N of the phenanthridinyl arms. This lower $^{3}J_{PtH}$ value is consistent with coordination to Pt(IV) in a pseudo-octahedral environment, as square-planar Pt(II) complexes usually display stronger Pt-H coupling compared to 6-coordinate Pt(IV).[25,26]

Substitution of the chlorido ligand of ^{CF3}**L**PtCl with L-type donors was then undertaken to increase the solubility of the subsequent salts in polar solvents. In particular, ^{CF3}**L**PtCl was reacted with an excess of either pyridine (py) or 4-(dimethylamino)pyridine (DMAP) in the presence of $AgPF_6$. Recrystallization from acetone and diethyl ether enabled isolation of [^{CF3}**L**Pt(py)]PF_6 and [^{CF3}**L**Pt(DMAP)]PF_6 as spectroscopically pure yellow powders in 60% and 94% yield, respectively. Consistent with the stronger donor ability of the *para*-substituted DMAP, the fully intact cationic component could be observed by HRMS for [^{CF3}**L**Pt(DMAP)]$^+$, while the major peaks in the spectrum of [^{CF3}**L**Pt(py)]PF_6 corresponded to the complex with loss of pyridine, [^{CF3}**L**Pt]$^+$, with signals for [^{CF3}**L**Pt(py)]$^+$ appearing with *ca.* 10^6 × lower intensity. An increase in solubility was noticeable for [^{CF3}**L**Pt(py)]PF_6 and [^{CF3}**L**Pt(DMAP)]PF_6 compared with ^{CF3}**L**PtCl and both salts are readily soluble in acetone. Multinuclear (^{1}H, ^{13}C, ^{19}F) NMR spectroscopy confirmed installation of the new *N*-donor ligand with the peaks for the additional ligand accompanying ^{19}F signals for a PF_6^- counterion and appearing with appropriate integrations.

An acetylido derivative ^{tBu}**L**Pt(C≡C-C_6H_4-*t*Bu) was also prepared. Adding a mixture of 4-*tert*-butylphenylacetylene (HC≡C-C_6H_4-*t*Bu) and sodium methoxide as base in methanol to a methanol/dichloromethane (4:1, v/v) solution of ^{tBu}**L**PtCl and stirring under ambient conditions for 24 h led to ~70% conversion (^{1}H NMR). Performing the reaction at slightly elevated temperature (50 °C) and resubmitting the isolated reaction mixture to the reaction conditions with additional equivalents of acetylene helped boost conversion, giving the acetylido product in 78% yield. As with [^{CF3}**L**Pt(DMAP)]$^+$, the intact molecular ion, [^{tBu}**L**Pt(C≡C-C_6H_4-*t*Bu)]$^+$, is observed by HR-MS. The *trans* influence of the cyclometallating ligand is thus balanced by the binding strength of the co-ligand (pyridine, DMAP or acetylido). As pyridine is the weakest binding of the three, pyridine detachment is more prominently observed in the gas-phase compared with the stronger σ-donor DMAP or the anionic acetylido which bears an additional electrostatic attraction to the Pt(II) center.

Solid-State Structures

The structures of ^{tBu}**LH**, three of the Pt(II) complexes and the Pt(IV) species were determined in the solid-state by X-ray diffraction. Single crystals of ^{tBu}**LH** were grown at -15 °C from a methanol solution (Figure S1; see SI for further discussion). Crystals of the platinum complexes suitable for analysis were grown by vapor diffusion into solutions of the complexes (see Experimental Section). The structures (Figure 2 and Table 1) confirm the expected connectivity, and in each case, short C=N (N1-C1/N2-C21) bonds are evident, consistent with the 'imine-like' biphenyl resonance character typical of phenanthridine's tricyclic fused ring system.[27] The structure of ^{tBu}**L**Pt(C≡C-C_6H_4-*t*Bu) confirmed the replacement of the chlorido ligand by 4-(*tert*-butyl)phenylacetylido, although the diffraction data indicated the presence of residual co-crystallized ^{tBu}**L**PtCl in the sample analyzed (around 5%). The Pt-C bond length in ^{CF3}**L**Pt(IV)Cl_3 [Pt1-C18 = 2.006(6) Å] is slightly longer than the Pt(II)-C bonds [^{tBu}**L**PtCl: C(16)-Pt(1) = 1.979(13) Å; [^{CF3}**L**Pt(pyr)][PF_6]: Pt1-C16 = 1.962(4) Å] and consistent with literature reports on Pt(II) vs. Pt(IV).[28–30]

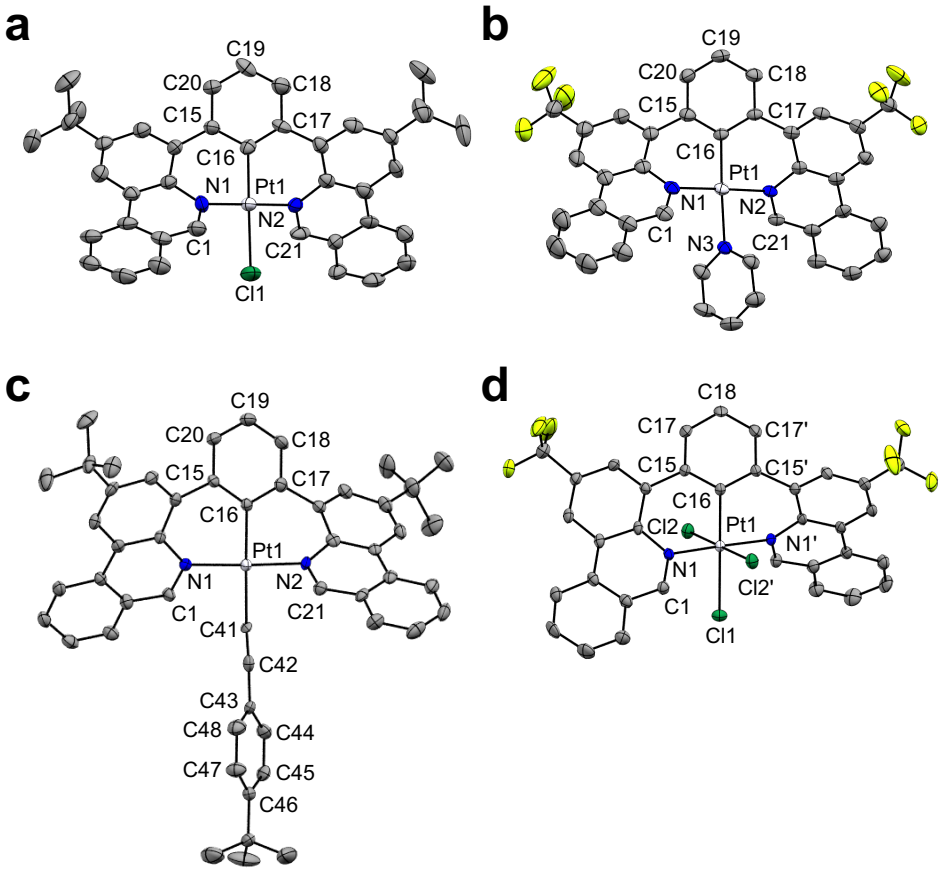

Figure 2. Solid-state structure of (a) ^{tBu}**L**PtCl, (b) [^{CF3}**L**Pt(py)]PF_6, (c) ^{tBu}**L**Pt(C≡C-C_6H_4-*t*Bu) and (d) ^{CF3}**L**$PtCl_3$ with thermal ellipsoids shown at 50% probability levels. Hydrogen atoms, co-crystallized solvent molecules and counterions omitted for clarity.

Table 1. Bond lengths (Å), bond angles (º), and torsional angles (º) of selected Pt complexes.

Parameter	$^{t\mathrm{Bu}}$**L**PtCl	[$^{\mathrm{CF3}}$**L**Pt(py)]PF_6	$^{t\mathrm{Bu}}$**L**Pt(C≡C-C_6H_4-*t*Bu)	Pt(dqb$^{\mathrm{Me,Me}}$)Cl[a]	Pt(dpyb)Cl[b]	$^{t\mathrm{Bu}}$**L**$PtCl_3$
Pt-$N_{Ar,1}$ / Å	2.018(10)	2.024(5)	2.036(4)	2.035(3)	2.041(6)	2.037(3)
Pt-$N_{Ar,2}$ / Å	2.019(10)	2.021(3)	2.030(4)	2.035(3)	2.033(6)	2.037(3)
Pt-C_{Ar} / Å	1.979(13)	1.962(5)	1.994(5)	1.992(5)	1.907(8)	2.006(6)
Pt-*X*[c] / Å	2.403(4)	2.125(4)	2.059(8)	2.451(1)	2.417(2)	2.456(2)
$N_{Ar,1}$-Pt-$N_{Ar,2}$ / °	179.3(4)	177.6(2)	177.2(2)	177.8(2)	161.1(2)	178.6(2)
C_{Ar}-Pt-X [c] / °	178.4(4)	176.4(2)	178.7(3)	180.0	179.0(2)	180.0
C_{Aryl}-Pt-$N_{Ar,1}$ / °	90.2(5)	90.7(2)	89.2(2)	91.1(1)	80.9(3)	90.7(1)
C_{Aryl}-Pt-$N_{Ar,2}$ / °	90.3(5)	90.2(2)	88.8(2)	91.1(1)	80.1(3)	90.7(1)
$N_{Ar,1}$-$C_{C=N,1}$-$C_{C=N,2}$-$N_{Ar,2}$ torsional angle / °	53.7(10)	51.0(4)	55.2(5)	46.2(3)	2.0(7)	53.2(4)
τ_4	0.016	0.043	0.029	0.02	0.14	*n/a*

[a] dqb$^{\mathrm{Me,Me}}$ = 4,6-dimethyl-1,3-di(8-quinolyl)benzene. Data from reference [18].
[b] Data from reference [31].
[c] *X* = coordinating atom of *trans* co-ligand (*X* = Cl in each case except the acetylido and pyridine complexes for which *X* = C and N respectively).

In all four compounds, the ligand twists to a remarkable degree to maintain a square-planar arrangement of the three ligating atoms of the *N^C⁻^N* unit and the monodentate ligand about the metal. The τ_4 values[32] calculated for the Pt center in the three four-coordinate complexes (^{tBu}**L**PtCl 0.016; [^{CF3}**L**Pt(py)]$^+$ 0.043; ^{tBu}**L**Pt(C≡C-C_6H_4-*t*Bu) 0.029) are very close to the ideal value of 0.0 for a square-planar geometry, as are those of the optimized structures (Table S4), thanks to the N-Pt-N and C-Pt-X angles being so close to 180° (Figure 3).

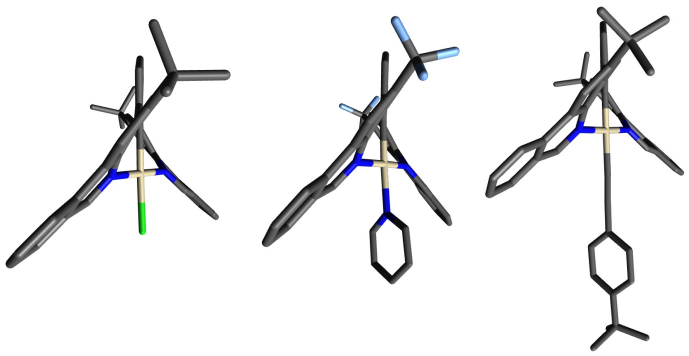

	^{tBu}**L**PtCl	[^{CF3}**L**Pt(py)]$^+$	^{tBu}**L**Pt(C≡CAr^{tBu})
Interplanar angle / °	40.1	37.8	44.0
N-Pt-N / °	179.3(4)	177.6(2)	177.2(2)
τ_4	0.016	0.043	0.029

Figure 3. View of solid-state structures of ^{tBu}**L**PtCl, [^{CF3}**L**Pt(py)]PF_6 and ^{tBu}**L**Pt(-C≡C-C_6H_4-*t*Bu) highlighting the twist in the tridentate ligand chelate while maintaining square-planar geometry at the metal center. Interplanar angles are the average of the two angles between the planes of the phenanthridine and the central phenyl ring.

Photophysical Properties

The absorption spectra of the Pt(II) complexes are shown in Figure 4 together with that of Pt(dqb)Cl, grouped to aid comparison, with data compiled in Table 2. The spectra of the complexes are qualitatively similar to one another, with high energy bands (300-350 nm) consistent with the presence of benzannulated phenanthridinyl ligand arms with energetically accessible, vacant π* orbitals.[20] Compared

with related complexes of *N*^*N*–^*N*-type diarylamido pincer ligands bearing phenanthridinyl donors, which present strong, defined absorption bands at ~500 nm and are deep red in color, the lowest energy features of the *N*^*C*–^*N*-supported complexes appear as shoulders at ~400 nm, consistent with the yellow color of the complexes. Such bands, absent in spectra of the proligands, are likely due to $d_{Pt} | \pi_L \rightarrow \pi^*_L$ charge-transfer states that arise from metallation (*vide infra*).[33]

Comparing the spectra of $^{t\mathrm{Bu}}$**L**PtCl with the quinoline analogue Pt(dqb)Cl in the first instance (Figure 4a), the lowest-energy absorption band is somewhat blue-shifted in the former, contrary to what might be expected intuitively based on the notion of more extended π conjugation leading to lower-energy excited states. We return to this point later. The introduction of the acetylido ligand leads to a small red-shift and longer low-energy tail (Figure 4a), consistent with the σ-donating nature of the acetylido raising the energy of filled metal orbitals involved in the CT state. There is also a small red-shift on going from $^{t\mathrm{Bu}}$**L**PtCl to $^{\mathrm{CF3}}$**L**PtCl, which can be rationalized in terms of the stabilization of the ligand π* orbitals by the electron-withdrawing CF_3 groups. A similarly slight shift to lower energy of the lowest absorption manifold is seen for Fe(II) complexes of CF_3 versus *t*Bu-substituted phenanthridine-containing diarylamido ligands.[34] The replacement of the chlorido ligand by pyridine or DMAP shifts λ_{max} to shorter wavelength (Figure 4b), consistent with the change from an anionic to neutral donor stabilizing the filled metal orbitals. The effect is evidently partially offset by the electron-donating NMe_2 group in the DMAP complex, with λ_{max} clearly in the order $^{\mathrm{CF3}}$**L**Pt(py) < $^{\mathrm{CF3}}$**L**Pt(DMAP) < $^{\mathrm{CF3}}$**L**PtCl.

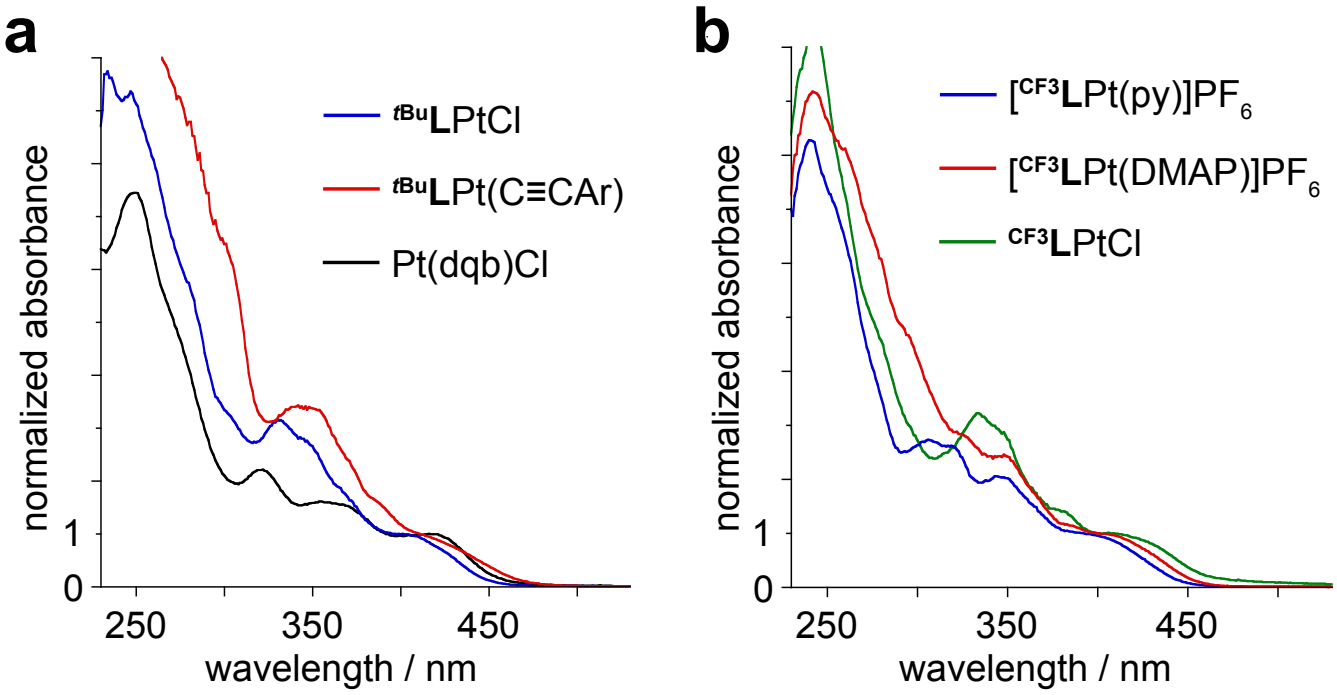

Figure 4. UV-Vis absorption spectra of (a) ^{tBu}**L**PtCl and its acetylido derivative, together with the quinolyl analogue Pt(dqb)Cl for comparison; (b) ^{CF3}**L**PtCl and its pyridyl and DMAP derivatives, in CH_2Cl_2 at 295 K in each case. Spectra are normalized to the longest wavelength feature, in each case.

Table 2. Absorption and Emission Data of Pt complexes[a]

Complex	Absorption λ_{max}/nm (ε / 10^3 M^{-1} cm^{-1})	Emission λ_{max}/nm	Φ_{lum} [b]	τ / μs [c]	k_r / 10^3 s^{-1} [d]	$\sum k_{nr}$ / 10^3 s^{-1} [d]	k_Q^{O2} / 10^8 M^{-1} s^{-1} [e]	Emission [f] 77 K	
								λ_{max}/nm	τ/μs
^{CF3}**L**PtCl	243 (73.5), 333 (21.6), 380 (9.12), 408 (6.25)	575(sh), 607	0.09 ± 0.02	16 ± 2 [1±0.1]	6	60	5	573, 613[g]	20
^{tBu}**L**PtCl	248 (68.7), 332 (37.7), 404 (11.8)	583(sh), 610	0.08 ± 0.02	19 ± 2 [1±0.1]	4	50	4	548, 593, 643	41
[^{CF3}**L**Pt(py)]PF_6	242 (89.5), 307 (41.8), 346 (34.7), 399 (15.2)	572(sh), 605	0.06 ± 0.02	18 ± 2 [1±0.1]	3	50	5	553, 595, 643	26
[^{CF3}**L**Pt(DMAP)]PF_6	243 (84.8), 345 (sh, 22.5), 407 (8.92)	576(sh), 610	0.05 ± 0.01	18 ± 2 [1±0.1]	3	50	5	560, 603	33
^{tBu}**L**Pt(C≡C-C_6H_4-*t*Bu)	347 (29.1) 427 (sh, 6.77)	585(sh), 612	0.02 ± 0.01	2.2 ± 0.2 [0.6±0.1]	7	400	6	560, 604	31
Pt(dqb)Cl [h]	320 (67.5), 356 (49.9), 420 (31.5)	611(sh), 645	1.6	14 [i]	1	70	[i]	575, 626, 676	28

[a] In degassed CH_2Cl_2 at 295 K, except where indicated otherwise. [b] Measured in degassed solution using $[Ru(bpy)_3]Cl_{2(aq)}$ as the standard; estimated uncertainty in Φ is ±20% of the reported values. [c] Luminescence lifetimes in degassed solution; corresponding values in air-equilibrated solution are given in square parentheses; estimated uncertainty is ±10% of the reported values. [d] Radiative k_r and nonradiative $\sum k_{nr}$ rate constants estimated from the quantum yield and lifetime, assuming that the emissive state is populated with unit efficiency upon light absorption, through the relationships $k_r = \Phi/\tau$; $k_{nr} = (1 - \Phi)/\tau$. Values are given to one significant figure only, reflecting the intrinsic uncertainty in experimental Φ and τ values. [e] Bimolecular Stern−Volmer constant for quenching by molecular oxygen, estimated from the lifetimes in degassed and air-equilibrated solution and assuming $[O_2]$ = 2.2 mmol dm^{-3} in CH_2Cl_2 at atmospheric pressure of air. [f] In diethyl ether / isopentane / ethanol (2:2:1 v/v). [g] The 77K spectrum is consistently poor for this complex, likely due to low solubility in the frozen glass. [h] Data for Pt(dqb)Cl are from ref.[14] [i] Emission is too weak for the luminescence lifetime of this complex to be measured under air-equilibrated conditions.

All of the complexes are luminescent in degassed solution at room temperature, emitting orange light with broad, unstructured profiles centered at ~610 nm (spectra of selected complexes are shown in Figure 5 and data for all are compiled in Table 2). A shoulder to the high-energy side of the maximum in each case hints at some vibrational structure with the 0,0 component being somewhat less intense than the 0,1 (or higher) vibrational levels. Indeed at 77 K (Figure 5b), vibrational structure becomes well-resolved with a progression of around 1400 cm^{-1} typical of aromatic units, and the 0,1 component band seen to be the most intense. The emission is strongly red-shifted relative to that of Pt(dpyb)Cl (λ_{max} =

491 nm in CH_2Cl_2 at room temperature[13]), consistent with the more extended π conjugation of phenanthridine compared to pyridine. But the emission maxima are *blue*-shifted relative to the quinoline analogue Pt(dqb)Cl, despite the more extended π system of phenanthridine compared to quinoline (λ_{max} = 645 and 610 nm for Pt(dqb)Cl[14] and $^{t\mathrm{Bu}}$**L**PtCl respectively). This follows previously reported trends of counter-intuitive, hypsochromic shifts in emission energy for transition metal complexes of phenanthridinyl-containing ligands.[35,36,19,20] There is a very small blue-shift in the emission upon changing from a *t*Bu to a CF_3 substituent in the phenanthridine, and essentially no effect on λ_{max} upon exchange of chlorido for the neutral or acetylido donors.

The quantum yields of luminescence in solution are quite respectable, reaching 0.09 ± 0.02 for $^{\mathrm{CF3}}$**L**PtCl in degassed CH_2Cl_2 at 295 K. These values rival that of the archetypal phosphorescent emitter $[Ru(bpy)_3]^{2+}$ (bpy = 2,2'-bipyridine) and are one to two orders of magnitude larger than those displayed by *N*^*N*^*N*-ligated Pt(II) complexes of related phenanthridine-based diarylamido ligands.[20] Apart from the acetylido derivative, the values are all considerably superior to that of Pt(dqb)Cl.[14] The luminescence decay profiles follow monoexponential (or approximately monoexponential) kinetics (see Figures S70-S74) with lifetimes (τ) in the range of 16 to 19 μs, with the exception of the acetylido complex for which τ is substantially shorter. There is no evidence of concentration quenching (at least for concentrations up to 3×10^{-4} M for $^{t\mathrm{Bu}}$**L**PtCl) nor excimer formation, in contrast to Pt(dpyb)Cl which shows clear excimer emission around 700 nm at concentrations in excess of about 4×10^{-5} M.[13]

The excitation spectra match the absorption spectra closely, showing that the emissive state is formed with something approaching unit efficiency. This allows the radiative (k_r) and non-radiative (Σk_{nr}) rate constants to be estimated from the lifetimes and quantum yields (Table 2, footnote d). There is a modest reduction in Σk_{nr} compared to Pt(dqb)Cl (as might be expected given the lower-energy emission from the latter) but what is more striking is the significantly higher k_r values in the phenanthridine complexes that serve to facilitate the emission. While improved, the radiative rates are still lower than

brighter emitters such as Pt(dpyb)Cl and *fac*-Ir(ppy)$_3$ (ppy = 2-phenylpyridine).[37] This suggests a lower participation of the metal in the excited state, diminishing the contribution of the metal's spin-orbit coupling in facilitating the formally spin-forbidden phosphorescence. The acetylido complex $^{t\mathrm{Bu}}$**L**Pt(C≡C-C$_6$H$_4$-*t*Bu) has the highest k_r value, which can probably be attributed to the σ-donating nature of the acetylido raising the energy of filled metal orbitals such that the metal participates more in the excited state; however, non-radiative decay is also increased in this complex, and to a much greater extent. Some insight into why this is so emerges from TD-DFT calculations that are discussed in the next section.

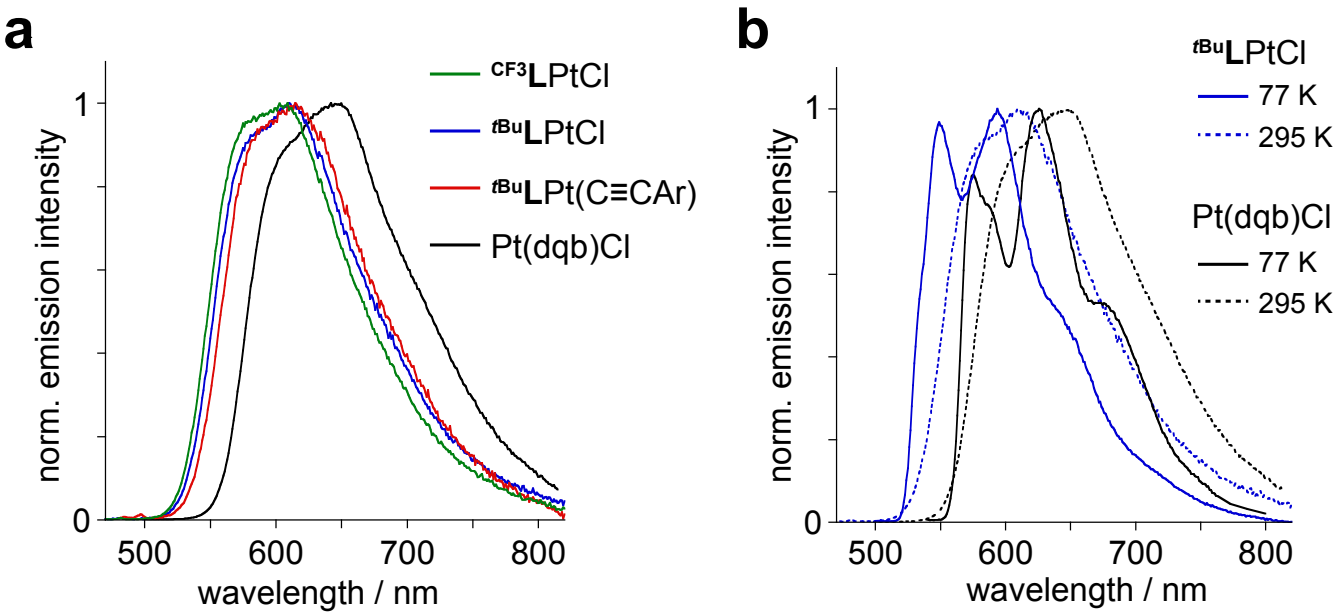

Figure 5. Photoluminescence spectra of (a) ^{CF3}**L**PtCl, $^{t\mathrm{Bu}}$**L**PtCl and its acetylido derivative, together with Pt(dqb)Cl for comparison in CH_2Cl_2 at 295 K in each case; (b) $^{t\mathrm{Bu}}$**L**PtCl and Pt(dqb)Cl at 77 K in a glass of diethyl ether / isopentane / ethanol (2:2:1 v/v) (solid lines), with the corresponding 295 K spectra re-shown as dashed lines for comparison.

Computational Analysis

Density functional theory (DFT) and time-dependent DFT (TD-DFT) modeling was performed to gain insight into the photophysics of the series. Ground-state molecular orbital (MO) energy level diagrams are shown in Figure 6. The highest occupied molecular orbital (HOMO) in each complex has considerable metal character (~20-30%), as well as orbital density on the cyclometallated phenyl ring and the co-ligand. The contribution of the co-ligand to the HOMO is smallest for $[^{CF3}\mathbf{L}Pt(py)]^+$ and largest for $^{tBu}\mathbf{L}Pt(C{\equiv}C\text{-}C_6H_4\text{-}t\text{Bu})$ and $[^{CF3}\mathbf{L}Pt(DMAP)]^+$. The chlorido co-ligands in $^{R}\mathbf{L}PtCl$ contribute an intermediate amount. The relative energy of this orbital does not track exactly with this contribution, as the acetylido complex has the most destabilized HOMO of the series while the energies of the HOMOs of $[^{CF3}\mathbf{L}Pt(DMAP)]^+$ and $[^{CF3}\mathbf{L}Pt(py)]^+$ are relatively similar and the lowest of the series.

Each complex has two closely spaced, low-lying vacant phenanthridine-based orbitals (LUMO, LUMO+1) which are π* in nature. As befits phenanthridinyl-type ligands, these orbitals are heavily localized on the C=N subunit of the tricyclic fused ring systems.[38] The biggest impact to the energies of these acceptor orbitals is the charge on the complex. The LUMO and LUMO+1 are lower in energy in $[^{CF3}\mathbf{L}Pt(L')]^+$ compared to the three neutral complexes. For $^{R}\mathbf{L}PtCl$ (R = *t*Bu, CF_3), introducing an electron-withdrawing group on phenanthridine stabilizes both the occupied and unoccupied frontier MOs. A larger stabilization is seen in the LUMO ($^{CF3}\mathbf{L}PtCl$: E_{LUMO} = -2.37 eV; $^{tBu}\mathbf{L}PtCl$: E_{LUMO} = -2.10 eV; ΔE_{LUMO} = -0.27 eV) and LUMO+1 ($^{CF3}\mathbf{L}PtCl$: E_{LUMO+1} = -2.35 eV; $^{tBu}\mathbf{L}PtCl$: E_{LUMO+1} = -2.09 eV; ΔE_{LUMO} = -0.26 eV) of $^{CF3}\mathbf{L}PtCl$ when compared to the HOMO ($^{CF3}\mathbf{L}PtCl$: E_{HOMO} = -6.14 eV; $^{tBu}\mathbf{L}PtCl$: E_{LUMO} = -5.96 eV; ΔE_{LUMO} = -0.18 eV), reproducing the shift to lower energy of λ_{max} observed by UV-Vis spectroscopy. This is consistent with what has been observed for CF_3-containing luminescent iridium(III) complexes of cyclometallated ligands in which both the HOMO and LUMO are stabilized, but the latter more so, inducing similar bathochromic shifts.[39]

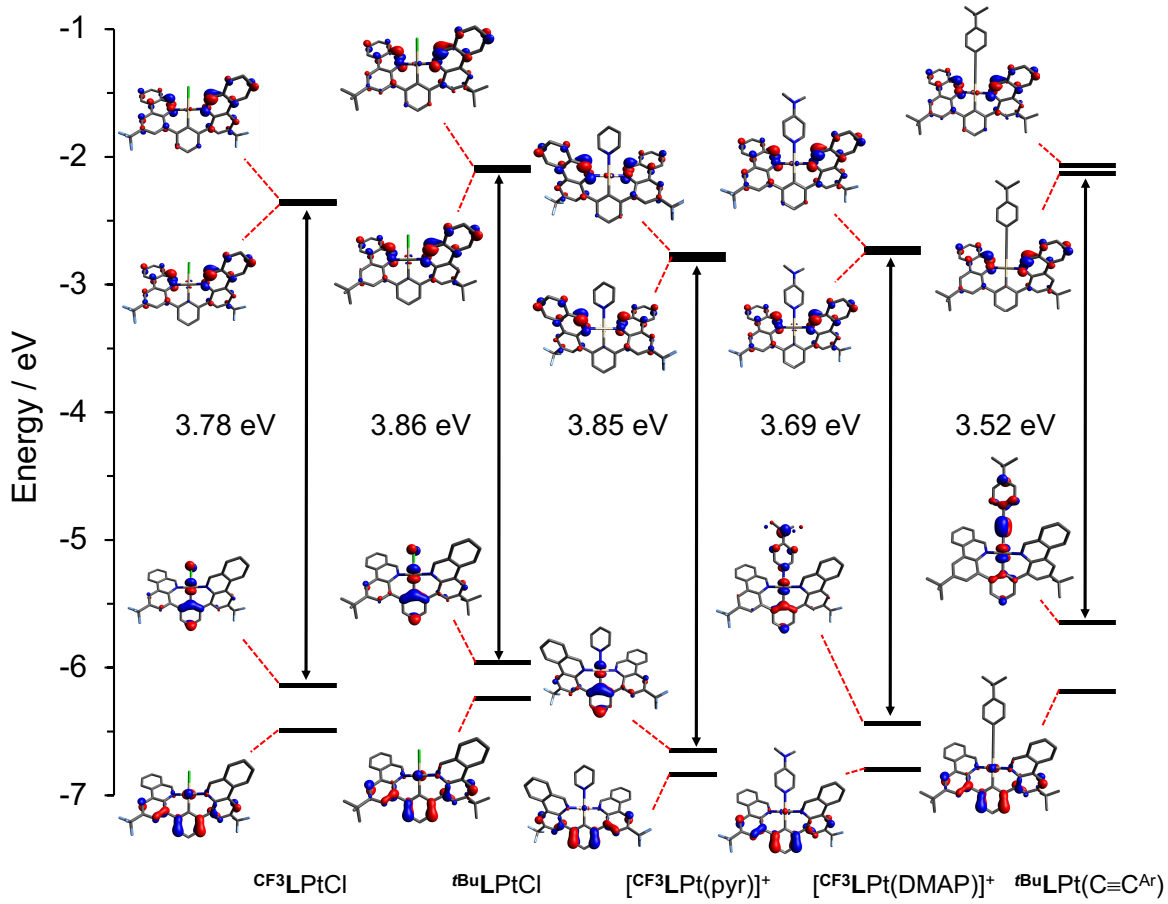

Figure 6. Molecular orbital diagram of selected orbitals and their energies (RIJCOSX-ZORA-SMD-PBE0-D3(BJ)/def2-TZVP+SARC-ZORA-TZVP//SMD-M06L-D3(BJ)/def2-SVP; isosurface = 0.05).

For the lowest energy absorption manifold, $[d_{Pt}+\pi(C_{aryl})+\pi(\text{co-ligand})]\rightarrow\pi^*(\text{phenanthridine})$ charge-transfer character is evident from both the MO diagrams and population analysis (see SI). Time-dependent density functional theory (TDDFT) simulations accurately reproduce the experimental spectra. A number of closely spaced absorptions are responsible for the higher energy features, but the low energy shoulder arises almost exclusively from strong HOMO→LUMO+1 transitions. This contrasts with the character of the lowest energy absorption of Pt(dqb)Cl which is mainly HOMO→LUMO in nature.[14] The LUMO and LUMO+1 isosurfaces are nearly identical and both have significant orbital density on the C=N subunit of the phenanthridinyl arms that is π* in character, but with differing

symmetry with respect to the two ligand arms: the two π*(C=N) orbital fragments are antisymmetric with rotation about the pseudo-C_2 molecular axis in the LUMO, and symmetric in the LUMO+1. The HOMO, with contributions from the Pt(d_{yz}), Cl(p_y) and aryl π-type orbitals, is also antisymmetric with respect to C_2 rotation. Accordingly, for the most symmetric species (e.g., $^{\mathbf{R}}$**L**PtCl), the HOMO→LUMO excitation has a much smaller transition dipole compared to the HOMO→LUMO+1 transition, and the oscillator strength of the former is negligibly low (see SI for further discussion). For Pt(dqp)Cl, DFT calculations show the LUMO to be more delocalized about the smaller quinolinyl π-system, alleviating symmetry concerns.[14] Indeed, when the chlorido ligands in $^{\mathbf{R}}$**L**PtCl are exchanged for larger ancillary ligands, the pseudo-C_2 symmetry of the complexes is lifted further and the HOMO→LUMO transition is turned on with increasing intensity: for [$^{\mathbf{CF3}}$**L**Pt(DMAP)]$^+$ the HOMO→LUMO transition is ~1% of the height of the HOMO→LUMO+1 transition, while for $^{t\mathbf{Bu}}$**L**Pt(C≡C-C_6H_4-*t*Bu) this transition is about 50% as intense as the HOMO→LUMO+1 transition and both excitations contribute strongly to the lowest-energy absorption. In any case, the low energy transitions can be assigned as charge-transfer (CT) in nature as the occupied frontier orbitals are heavily based on the chelating carbanionic aryl ring and platinum center, with some additional contribution from the co-ligand.

While the character of the transitions and HOMO-LUMO gap of the platinum complexes differ, the emission profiles of all the complexes are nearly identical despite changes to the co-ligand and charge. This implies that the emissive state has significant ligand character at the expense of metal involvement, in line with the aforementioned discussion of k_r. Comparing the geometries and bonding parameters of the optimized ground-state (S_0) and lowest-lying triplet state (T_1), only one bond to Pt (Pt-N) is seen to elongate in the excited state (average Δd(Pt-N) = +0.032 Å). The remaining Pt-N bond (average Δd(Pt-N): -0.25 Å), Pt-C bond (average Δd(Pt-C): -0.012 Å) and the Pt bond to the ancillary ligand (Pt-X) *contract* slightly (Table S15). Only the Pt-N_{pyr} bond in [$^{\mathbf{CF3}}$**L**Pt(py)]$^+$ is left unchanged in the excited state. Metal-centered states in which a strongly antibonding metal–ligand orbital is populated should

result in elongation of metal–ligand bonds. These observations support the idea – central to the use of cyclometallated aryl-heterocycle ligands – that by combining a strongly donating ligand with good π-acceptors, undesirable MC excited states will be destabilized in favor of radiative CT states. The biggest difference between ground-state and excited-state geometries is observed for $^{t\mathrm{Bu}}$**L**Pt(C≡C-C_6H_4-*t*Bu). In the optimized T_1 structure for this complex, a major change in the C-Pt-C bond angle is observed (S_0: 179.9°; T_1: 154.7°; ΔC-Pt-C: 25.2°) compared with the rest of the series (average ΔC-Pt-X: 2.2°; X = coordinating atom of *trans* co-ligand). This change may explain the higher Σk_{nr} and hence lower emission efficiency of this complex, as excited state distortion invariably promotes non-radiative vibronic deactivation.

As seen with related *N^N⁻^N*-ligated Pt(II) complexes of phenanthridine-containing diarylamido ligands,[19,20] the C=N sub-unit of the phenanthridinyl ligand arms buffer against more widespread molecular distortions in the optimized T_1 structures (Figures S14-S20). Namely, the elongation of the C=N bond on one ligand arm is the most pronounced distortion in all complexes, aside from $^{t\mathrm{Bu}}$**L**Pt(C≡C-C_6H_4-*t*Bu) in which both the C=N sub-unit and Pt-$C_{acetylido}$ bonds are impacted to similar degrees [Δ(C=N) = 0.065 $^{t\mathrm{Bu}}$**L**PtCl; 0.055 $^{\mathrm{CF3}}$**L**PtCl; 0.060 [$^{\mathrm{CF3}}$**L**Pt(pyr)]$^+$; 0.059 Å [$^{\mathrm{CF3}}$**L**Pt(DMAP)]$^+$; 0.043 $^{t\mathrm{Bu}}$**L**Pt(C≡C-C_6H_4-*t*Bu)]. This phenanthridinyl donor is the one that undergoes a Pt-N bond contraction in the excited state, consistent with introduction of $Pt^{\delta+}$-$N^{\delta-}$ charge-transfer character. The localization of the π-accepting character of phenanthridine at the C=N sub-unit accentuates the $N^{\delta-}$ character in the T_1 state. In comparison, the same C=N bond elongates to a much smaller degree in the optimized T_1 state of Pt(dpyb)Cl (Δ(C=N) = 0.007 Å), and the corresponding reduction in the Pt-N distance is smaller (0.013 Å).

The similarities between the experimental emission profiles can be reproduced computationally by calculating the difference in energy of the optimized T_1 state (E_{T1}) and the single-point energy of the structure with this optimized T_1 geometry and singlet multiplicity ($E_{T1@S0}$): only minor differences in the

so-determined calculated phosphorescence energy ($E_{vert,phos}$) are predicted (Table S16). The fidelity of the emission profiles can be further understood by visualization of the spin density (Figure S21). This shows that all the complexes have very similar character in their lowest-lying triplet excited states, with what appears to be seemingly no change depending on the phenanthridine R group and only minor dependence on the ancillary ligand. In general, these plots indicate spin density in the T_1 state on one of the phenanthridine moieties along with the platinum center and, to a smaller degree, the chelating aryl ring. The calculated T_1 energies are intermediate between those of Pt(dpyb)Cl and Pt(dqb)Cl, in line with the observed differences in emission wavelength. Similarly, the energetic cost of geometry relaxation of the T_1 state to the S_0 state, which can be estimated by calculating the corresponding relaxation energy (λ_T),[40] is lowest for the brightest emitter (Pt(dpyb)Cl, λ_T = 0.23 eV) and highest for the weakest emitter ($^{t\mathbf{Bu}}$**L**Pt(C≡C-C_6H_4-*t*Bu), λ_T = 0.60 eV), with intermediate values obtained for the remaining compounds (~0.3 eV).

Conclusions

In summary, 1,3-di(4-phenanthridinyl)benzenes $^{\mathbf{R}}$**LH** have been shown to form platinum(II) complexes of the type $^{\mathbf{R}}$**L**PtX and [$^{\mathbf{R}}$**L**PtL']$^+$ that are quite brightly photoluminescent in the orange region of the spectrum. Their emission is blue-shifted compared to a previously described quinolyl analog, Pt(dqb)Cl,[14] despite the more extended π conjugation of the phenanthridine compared to quinoline units, a result that is in line with a series of recent studies on phenanthridine-based complexes which have shown how site-selective benzannulation can be used to destabilize triplet excited states.[19,36] We trace this effect using DFT and TDDFT to the unique orbital character of the phenanthridinyl ligand arms which serves to localize the acceptor orbitals (e.g., LUMO, LUMO+1) particularly at the C=N sub-unit; accordingly, the nature of the substituent R in the 2-position has rather little influence on the emission properties. The chlorido co-ligand of the initially formed $^{\mathbf{R}}$**L**PtCl complexes can be readily exchanged for other neutral and anionic donor ligands, mostly without compromising the emission. While the

quantum yields reported here trail those of very strongly emissive neutral Pt(II) complexes of tridentate, dianionic 2,6-*bis*(1H-1,2,4-triazol-5-yl)pyridine-based *N*$^{-}$^*N*^*N*$^{-}$-ligands,[41] for example, this study shows how site-selective benzannulation can overcome the detrimental effect of enlarging the chelate ring-size in *N*^*C*$^{-}$^*N*-supported Pt(II) emitters. Notwithstanding the generally favorable impact of arylacetylido co-ligands on the photophysical properties of platinum(II) complexes of diimine and triimine ligands and of some cyclometalated ligands,[42] the introduction of an acetylido as the monodentate ligand in this instance is disadvantageous despite favorably increasing metal character in the excited state, due to greatly increased non-radiative decay.

EXPERIMENTAL

General Information

Air-sensitive manipulations were carried either in a N_2-filled glove box or using standard Schlenk techniques under Ar. 4-Bromo-2-(trifluoromethyl)phenanthridine[34] and 4-bromo-2-(*tert*-butyl)phenanthridine[20] were synthesized according to literature procedures. 1,3-Benzene diboronic acid (Combi Blocks), *tetrakis*(triphenylphosphine)palladium (Millipore Sigma), potassium tetrachloridoplatinate (Alfa Aesar), pyridine (Fisher Scientific), 4-(dimethylamino)pyridine (Alfa Aesar), silver (I) hexafluorophosphate (TCI America), 4-*tert*-butyl-phenylacetylene (Sigma Aldrich) and other common reagents were purchased from commercial suppliers and used without further purification. For moisture-sensitive manipulations, organic solvents were dried and distilled using appropriate drying agents. 1- and 2D NMR spectra were recorded on Bruker Avance 300 MHz or Bruker Avance – III 500 MHz spectrometers. ^{1}H, and ^{13}C NMR spectra were referenced to residual solvent peaks. High resolution mass spectra (HRMS) were recorded using a Bruker microOTOF-QIII mass spectrometer. Elemental analyses were carried out at Micro-Analysis, Inc. (Wilmington, DE) and Guelph Chemical Laboratories Ltd. (Guelph, CA).

Synthesis of 1,3-*bis*(4-(2-trifluoromethyl)phenanthridinyl))benzene ^{CF3}LH: A thick-walled Teflon-stoppered flask was charged with 4-bromo-2-(trifluoromethyl)phenanthridine (0.570 g, 1.80 mmol), 1,3-benzene diboronic acid (0.150 g, 0.880 mmol), toluene (4.4 mL) and ethanol (8.8 mL). *Tetrakis*(triphenylphosphine)palladium (0.051 g, 0.044 mmol) was then added, followed by additional toluene (4.4 mL) and a solution of sodium carbonate (0.930 g, 8.79 mmol) in water (4.4 mL). Argon was bubbled through the solution for 10 min while stirring. The flask was then sealed and stirred for 72 h in an oil bath set at 130 °C. The solution was then cooled to room temperature and dichloromethane (~200 mL) was added. The resulting organic layer was washed with deionized water (50 mL) followed by a saturated solution of sodium chloride (2 x 50 mL). The organic layer was collected, dried over sodium sulfate, filtered and volatiles were removed *in vacuo*. The residue was taken up in ethanol and the mixture heated to boiling temperature, then filtered while hot over Celite. Any filtered soluble material was pulled through the filter with ~75 mL CH_2Cl_2 and dried to isolate a spectroscopically pure white solid. Yield = 0.340 g (68%). ^{1}H NMR ($CDCl_3$, 300 MHz, 22°C): δ 9.42 (s, 2H; C_1-*H*), 8.90 (d, $^4J_{HH}$ = 0.7 Hz, 2H; C_{13}-*H*), 8.71 (d, $^3J_{HH}$ = 8.3 Hz, 2H; C_6-*H*), 8.11 (m, 4H; $C_{3,11}$-*H*), 8.05 (t, $^4J_{HH}$ = 1.5 Hz, 1H; C_{16}-*H*), 7.96 (ddd, $^3J_{HH}$ = 8.4, 7.3, $^4J_{HH}$ = 1.3 Hz, 2H; C_5-*H*), 7.82 (m, 4H; $C_{4,17}$-*H*), 7.71 ppm (dd, $^3J_{HH}$ = 8.4, 7.0 Hz, 1H; C_{18}-*H*). ^{13}C{^{1}H} NMR ($CDCl_3$, 75 MHz, 22 °C): δ 155.3 (C_1), 142.8 (C_9), 138.8 (C_{15}), 133.2 (C_{16}), 132.6 (C_8), 131.8 (C_5), 130.5 (C_{17}), 129.1 (C_3), 128.7 (C_{12}), 128.6 (C_4), 128.3 (C_2), 128.0 (C_{18}), 126.5 (C_7), 126.2 (q, $^4J_{FC}$ = 3.1 Hz; C_{11}), 124.5 (C_{10}), 122.3 (C_6), 119.4 ppm (q, $^4J_{FC}$ = 4.1 Hz; C_{13}). A resonance for C_{14} could not resolved in the ^{13}C{^{1}H} NMR spectrum. ^{19}F{^{1}H} NMR ($CDCl_3$, 282 MHz, 22 °C): δ -61.8 ppm. HR-MS (APCI-TOF) m/z: $[M + H]^+$ calculated for $[C_{34}H_{19}F_6N_2]^+$: 569.1447; found: 569.1483.

Synthesis of 1,3-bis(4-(2-tert-butylphenanthridinyl))benzene ^{tBu}LH: An identical procedure was followed as for **^{CF3}LH** using 4-bromo-2-(*tert*-butyl)phenanthridine (1.02 g, 1.60 mmol), 1,3-benzene diboronic acid (0.268 g, 1.60 mmol), toluene (8.0 mL) and ethanol (16 mL); *tetrakis*(triphenylphosphine)palladium (0.090 g, 0.081 mmol), additional toluene (8.0 mL), sodium carbonate (1.72 g, 16.0 mmol) and water (8.1 mL).

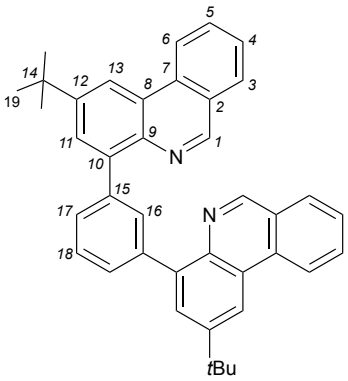

A spectroscopically pure brown solid was isolate by recrystallization in a solution of 9:1 methanol: water. Yield = 0.670 g (76%). ^{1}H NMR ($CDCl_3$, 300 MHz, 22 °C): δ 9.34 (s, 2H; C_1-*H*), 8.74 (d, $^{3}J_{HH}$ = 8.3 Hz, 2H; C_6-*H*), 8.66 (d, $^{4}J_{HH}$ = 2.1 Hz, 2H; C_{13}-*H*), 8.11 (t, $^{4}J_{HH}$ = 1.5 Hz, 1H; C_{16}-*H*), 8.05 (m, 4H; $C_{3,11}$-*H*), 7.88 (m, 4H; $C_{5,17}$-*H*), 7.72 (m, 3H; $C_{4,18}$-*H*), 1.58 ppm (s, 18H; C_{19}-*H*). ^{13}C{^{1}H} NMR ($CDCl_3$, 75 MHz, 22 °C): δ 152.6 (*C*$_1$), 149.6 (*C*$_{12}$), 141.5 (*C*$_9$), 140.5 (*C*$_8$), 140.2 (*C*$_{15}$), 133.0 (*C*$_{16}$), 133.0 (*C*$_7$), 130.7 (*C*$_5$), 130.2 (*C*$_{17}$), 129.0 (*C*$_3$); 128.8 (*C*$_{11}$), 127.4 (*C*$_{18}$), 127.3 (*C*$_4$), 126.4 (*C*$_2$), 124.0 (*C*$_{10}$), 122.1 (*C*$_6$), 117.3 (*C*$_{13}$), 35.5 (*C*$_{14}$), 31.7 ppm (*C*$_{19}$). HR-MS (APCI-TOF) m/z: $[M + H]^+$ calculated for $[C_{40}H_{37}N_2]^+$: 545.2951; found: 545.2921.

Synthesis of 1,3-bis(4-(2-trifluoromethylphenanthridinyl))benzene platinum chloride ^{CF3}LPtCl: A 100 mL Teflon-stoppered flask was charged with **^{CF3}LH** (0.050 g, 0.088 mmol), potassium tetrachloridoplatinate (0.044 g, 0.11 mmol), and glacial acetic acid (33 mL). The solution was degassed by 3 freeze-pump-thaw cycles. After refilling with argon, the flask was sealed and stirred in an oil bath set to 100 °C for 48 h. The resulting solution was cooled to room temperature, vacuum filtered, and the precipitate was washed with deionized water (~20 mL), pentane (~20 mL), and diethyl ether (~20 mL) resulting in a yellow powder. Yield = 0.060 g (85%). ^{1}H NMR (CD_2Cl_2, 500 MHz, 4096 scans, 22°C): δ 10.29 (s, $^{3}J_{PtH}$ = 45.7 Hz; C_1-*H*), 8.89 (s, 2H; C_{13}-*H*), 8.70 (d, $^{3}J_{HH}$ = 8.7 Hz, 2H; C_6-*H*), 8.51 (d, $^{4}J_{HH}$ = 1.4 Hz, 2H; C_{11}-*H*), 8.20 (d, $^{3}J_{HH}$ = 7.9 Hz, 2H; C_3-*H*), 8.14 (ddd, $^{3}J_{HH}$ = 8.3,

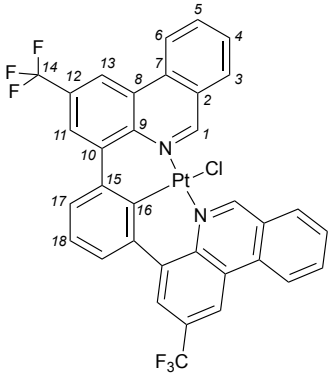

7.8, $^{4}J_{HH}$ = 1.2 Hz, 2H; C_5-*H*), 7.84 (ddd, $^{3}J_{HH}$ = 8.3, 7.5, $^{4}J_{HH}$ = 0.7 Hz, 2H; C_4-*H*), 7.66 (d, $^{3}J_{HH}$ = 7.7 Hz, 2H; C_{17}-*H*), 7.42 ppm (t, $^{3}J_{HH}$ = 7.7 Hz, 1H; C_{18}-*H*). $^{19}F\{^{1}H\}$ NMR ($CDCl_3$, 282 MHz, 22 °C): δ -62.2 ppm. The complex was too insoluble to acquire a meaningful ^{13}C NMR spectrum. HR-MS (APCI-TOF) m/z: $[M - Cl]^+$ calculated for $[C_{34}H_{17}F_6PtN_2]^+$: 762.0941; found: 762.0969. Anal. Calc. for $C_{34}H_{17}Cl_1F_6N_2Pt$: C, 51.17; H, 2.15; N, 3.51 %. Found: C, 50.91; H, 2.42; N, 3.19 %. This complex was found to be unstable in chlorinated solvents over extended periods of time, forming the oxidized octahedral Pt(IV) complex ^{CF3}**L**$PtCl_3$, as identified by single-crystal X-ray diffraction.

Synthesis of 1,3-bis(4(-2-*tert*-butylphenanthridinyl)benzene platinum chloride $^{t\mathrm{Bu}}$LPtCl: A 100 mL Teflon-stoppered flask was charged with $^{t\mathrm{Bu}}$**LH** (0.050 g, 0.092 mmol), potassium tetrachloridoplatinate (0.046 g, 0.11 mmol), and glacial acetic acid (34 mL). The solution was degassed by 3 freeze-pump-thaw cycles. After refilling with argon, the flask was sealed and stirred in an oil bath set to 100 °C for 48 h. The resulting solution was cooled to room temperature, filtered and the precipitate collected and washed with deionized water (~20 mL), pentane (~20 mL) and diethyl ether (~20 mL). A spectroscopically pure yellow powder was isolated. Yield = 0.056 g (79%). ^{1}H NMR ($CDCl_3$, 300 MHz, 22°C): δ 10.17 (s, $^{3}J_{PtH}$ = 46.2 Hz, 2H; C_1-*H*), 8.62 (d, $^{3}J_{HH}$ = 8.5 Hz, 2H; C_6-*H*), 8.52 (d, $^{4}J_{HH}$ = 1.5 Hz, 2H; C_{13}-*H*), 8.38 (d, $^{4}J_{HH}$ = 1.6 Hz, 2H; C_{11}-*H*), 8.07 (d, $^{3}J_{HH}$ = 7.9 Hz, 2H; C_3-*H*), 7.97 (t, $^{3}J_{HH}$ = 7.7 Hz, 2H; C_5-*H*), 7.66 (t, $^{3}J_{HH}$ = 7.5 Hz, 2H; C_4-*H*), 7.55 (d, $^{3}J_{HH}$ = 7.7 Hz, 2H; C_{17}-*H*), 7.35 (t, $^{3}J_{HH}$ = 7.7 Hz, 1H; C_{18}-*H*), 1.59 ppm (s, 18H; C_{19}-*H*). $^{13}C\{^{1}H\}$ NMR ($CDCl_3$, 75 MHz, 22 °C): δ 160.1 (C_1), 151.1 (C_{12}), 141.2 (C_{15}), 136.0 (C_{10}), 135.8 ($C_{9,29}$), 133.1 (C_5), 133.1 (C_2), 130.0 (C_3), 128.5 (C_{16}), 128.3 (C_4), 127.2 (C_{17}), 126.4 (C_7), 126.3 (C_{11}), 125.8 (C_{18}), 124.6 (C_8), 122.2 (C_6), 116.6 (C_{13}), 35.5 (C_{14}), 31.6 ppm (C_{19}). HR-MS (APCI-TOF) m/z: $[M - Cl]^+$ calculated for $[C_{40}H_{35}PtN_2]^+$: 738.2446; found: 738.2411.

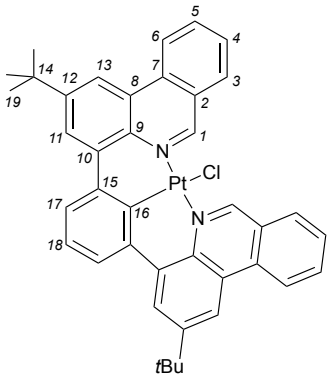

Synthesis of 1,3-*bis*(4-(2-trifluoromethylphenanthridinyl))benzene platinum pyridine hexafluoridophosphate [^{CF3}LPt(py)]PF_6: A round bottom flask was charged with ^{CF3}LPtCl (0.050 g, 0.063 mmol), pyridine (13 μL, 0.16 mmol) and dichloromethane (16 mL). The solution was stirred at room temperature and after 1 h, a solution of $AgPF_6$ (0.019 g, 0.076 mmol) in methanol (5.8 mL) was added. The reaction mixture was protected from light and stirred at room temperature overnight. The resulting AgCl was filtered off and solvent removed *in vacuo*. The product was recrystallized in a 1:2 mixture of diethylether and acetone, depositing a spectroscopically pure yellow powder. Yield = 0.037 g (60%). ^{1}H NMR ($(CD_3)_2CO$, 500 MHz, 22°C): δ 9.28 (d, $^4J_{HH}$ = 0.7 Hz, 2H; C_{13}-*H*), 9.15 (d, $^3J_{HH}$ = 8.4 Hz, 2H; C_6-*H*), 9.11 (s, 2H; C_1-*H*), 8.69 (d, $^4J_{HH}$ = 1.4 Hz, 2H; C_{11}-*H*), 8.27 (ddd, $^3J_{HH}$ = 8.4, 7.1, $^4J_{HH}$ = 1.3 Hz, 2H; C_5-*H*), 8.16 (m, 2H; C_{19}-*H*), 8.07 (tt, $^3J_{HH}$ = 7.7, $^4J_{HH}$ = 1.5 Hz, 1H; C_{21}-*H*), 7.93 (dd, $^3J_{HH}$ = 8.0, $^4J_{HH}$ = 0.8 Hz, 2H; C_3-*H*), 7.85 (ddd, $^3J_{HH}$ = 7.9, 7.1, $^4J_{HH}$ = 0.6 Hz, 2H; C_4-*H*), 7.78 (d, $^3J_{HH}$ = 7.8 Hz, 2H; C_{17}-*H*), 7.47 ppm (overlapped m, 3H; $C_{18,20}$-*H*). ^{13}C{^{1}H} NMR ($(CD_3)_2CO$, 126 MHz, 22 °C): δ 162.3 (*C*$_1$), 152.0 (*C*$_{19}$), 143.4 (*C*$_{15}$), 141.2 (*C*$_{21}$), 139.2 (*C*$_9$), 136.5 (*C*$_5$), 136.2 (*C*$_{10}$), 133.7 (*C*$_7$), 131.2 (q, $^2J_{FC}$ = 32.9 Hz; *C*$_{12}$), 131.2 (*C*$_4$), 130.6 (*C*$_3$), 129.2 (*C*$_{17}$), 128.3 (*C*$_{18}$), 128.2 (*C*$_{20}$), 127.6 (*C*$_2$), 126.7 (*C*$_8$), 124.3 (q, $^3J_{FC}$ = 3.0 Hz; *C*$_{11}$), 124.3 (*C*$_6$), 120.5 ppm (q, $^3J_{FC}$ = 4.1 Hz; *C*$_{13}$). Resonances for *C*$_{14}$ and *C*$_{16}$ were not resolved in the ^{13}C{^{1}H} NMR spectrum. ^{19}F{^{1}H} NMR ($(CD_3)_2CO$, 471 MHz, 22 °C): δ -62.5 (s, 6F; *F*$_{Phen}$), -71.8 (s, 3F; P*F*$_6$), -73.3 ppm (s, 3F; P*F*$_6$). ^{31}P{^{1}H} NMR ($(CD_3)_2CO$, 202 MHz, 22 °C): δ -144.3 ppm (sep, *P*F_6). HR-MS (APCI-TOF) m/z: $[M - pyr]^+$ calculated for $[C_{34}H_{17}F_6N_2Pt]^+$: 762.0941; found: 762.0905.

Synthesis of 1,3-bis(4-(2-trifluoromethylphenanthridinyl))benzene platinum (4-dimethylamino)pyridine hexafluoridophosphate [^{CF3}LPt(DMAP)]PF_6: A round bottom flask was charged with ^{CF3}LPtCl (0.050 g, 0.063 mmol), (4-dimethylamino)pyridine (0.019 g, 0.16 mmol) and dichloromethane (16 mL). The solution was stirred at room temperature and after one hour a solution of $AgPF_6$ (0.019 g, 0.076 mmol) in methanol (5.8 mL) was added. The reaction mixture was protected from light and stirred at room temperature overnight. Solid AgCl was then filtered off and the solvent removed *in vacuo*. The product was recrystallized in a 1:2 mixture of diethylether and acetone, depositing a spectroscopically pure yellow powder. Yield = 0.061 g (94%). ^{1}H NMR ($(CD_3)_2CO$, 500 MHz, 22°C): δ 9.29 (d, $^4J_{HH}$ = 0.7 Hz, 2H; C_{13}-*H*), 9.19 (m, 4H; $C_{1,6}$-*H*), 8.69 (d, $^4J_{HH}$ = 1.3 Hz, 2H; C_{11}-*H*), 8.29 (ddd, $^3J_{HH}$ = 8.4, 7.2, $^4J_{HH}$ = 1,2 Hz, 2H; C_5-*H*), 8.00 (d, $^3J_{HH}$ = 7.9 Hz, 2H; C_3-*H*), 7.89 (ddd, $^3J_{HH}$ = 7.8, 6.9, $^4J_{HH}$ = 0.6 Hz, 2H; C_4-*H*), 7.79 (d, $^3J_{HH}$ = 7.8 Hz, 2H; C_{17}-*H*), 7.49 (m, 2H; C_{19}-*H*), 7.44 (t, $^3J_{HH}$ = 7.7 Hz, 1H; C_{18}-*H*), 6.53 (m, 2H; C_{20}-*H*), 3.03 ppm (s, 6H; C_{22}-*H*). ^{13}C{^{1}H} NMR ($(CD_3)_2CO$, 126 MHz, 22 °C): δ 162.5 (*C*$_1$), 155.8 (*C*$_{21}$), 150.1 (*C*$_{19}$), 143.7 (*C*$_{15}$), 139.4 (*C*$_9$), 136.3 (*C*$_5$), 136.2 (*C*$_{10}$), 133.7 (*C*$_8$), 131.1 (*C*$_4$), 130.7 (*C*$_3$), 129.1 (*C*$_{17}$), 127.9 (*C*$_{18}$), 127.6 (*C*$_7$), 126.6 (*C*$_2$), 124.3 (overlapping peaks, *C*$_{6,11}$), 120.3 (q, $^3J_{FC}$ = 3.2 Hz; *C*$_{13}$), 109.3 (*C*$_{20}$), 39.3 ppm (*C*$_{22}$). Resonances for *C*$_{12}$, *C*$_{14}$ and *C*$_{16}$ were not resolved in the ^{13}C{^{1}H} NMR spectrum. ^{19}F{^{1}H} NMR ($(CD_3)_2CO$, 471 MHz, 22 °C): δ -62.5 (s, 6F; *F*$_{Phen}$), -71.9 (s, 3F; P*F*$_6$), -73.4 ppm (s, 3F; P*F*$_6$). ^{31}P{^{1}H} NMR ($(CD_3)_2CO$, 202 MHz, 22 °C): δ -144.3 ppm (sep, *P*F_6). HR-MS (APCI-TOF) m/z: $[M]^+$ calculated for $[C_{41}H_{27}F_6N_4Pt]^+$: 884.1786; Found: 884.1796.

Synthesis of 1,3-bis(4-(2-*tert*-butylphenanthridinyl))benzene 4-*tert*-butylphenylacetylene ^{tBu}LPt(-C≡C-C$_6$H$_4$-*t*Bu): A round bottom flask was charged with sodium methoxide (0.004 g, 0.065 mmol), 4-*tert*-butylphenylacetylene (12 µL, 0.065 mmol) and methanol (1 mL). The solution was then stirred at room temperature under nitrogen and after 30 min a suspension of $^{t\mathrm{Bu}}$**L**PtCl (0.050 g, 0.065 mmol) in a mixture of methanol (38 mL) and dichloromethane (10 mL) was added. The solution was stirred in an oil bath heated to 50 °C. After 24 h, the reaction mixture was cooled to room temperature and the solvent removed *in vacuo*. The resulting solid was washed with deionized water (~15 mL) and pentane (~15 mL) and then collected. The collected yellow-orange solid was resubmitted following the same procedure, leaving a spectroscopically pure yellow-orange powder. Yield = 0.047 g (81%). ^{1}H NMR ($CDCl_3$, 300 MHz, 22°C): δ 10.58 (s, $^3J_{PtH}$ = 58.6 Hz, 2H; C$_1$-*H*), 8.64 (d, $^3J_{HH}$ = 8.4 Hz, 2H; C$_6$-*H*), 8.52 (d, $^4J_{HH}$ = 1.8 Hz, 2H; C$_{13}$-*H*), 8.43 (d, $^4J_{HH}$ = 1.8 Hz, 2H; C$_{11}$-*H*), 7.98 (m, 4H; C$_{3,5}$-*H*), 7.68 (overlapped m, 4H; C$_{4,17}$-*H*), 7.36 (t, $^3J_{HH}$ = 7.7 Hz 1H; C$_{18}$-*H*), 7.09 (m, 4H; C$_{23,24}$-*H*), 1.60 (s, 18H; C$_{19}$-*H*), 1.25 ppm (s, 9H; C$_{27}$-*H*). ^{13}C{^{1}H} NMR ($CDCl_3$, 75 MHz, 22 °C): δ 162.9 (*C*$_1$), 150.8 (*C*$_{12}$), 147.9 (*C*$_{25}$), 142.8 (*C*$_{15}$), 137.6 (*C*$_{10}$), 136.4 (*C*$_9$), 135.3 (*C*$_{16}$), 133.3 (*C*$_7$), 132.8 (*C*$_5$), 131.0 (*C*$_{24}$), 129.4 (*C*$_3$), 128.2 (*C*$_4$), 127.0 (*C*$_{11}$), 126.7 (*C*$_2$), 126.6 (*C*$_{17}$), 125.8 (*C*$_{18}$), 125.4 (*C*$_{22}$), 124.9 (*C*$_8$), 124.8 (*C*$_{23}$), 122.3 (*C*$_6$), 116.4 (*C*$_{13}$), 107.9 (*C*$_{21}$), 83.5 (*C*$_{20}$), 35.5 (*C*$_{14}$), 34.6 (*C*$_{26}$), 31.6 (*C*$_{19}$), 31.4 ppm (*C*$_{27}$). HR-MS (APCI-TOF) m/z: [M + H]$^+$ calculated for [$C_{52}H_{48}N_2Pt$]$^+$: 896.3542; Found: 896.3530. As a minor impurity of $^{t\mathrm{Bu}}$**L**PtCl was observed co-crystallized with $^{t\mathrm{Bu}}$**L**Pt(C≡C-C$_6$H$_4$-*t*Bu) in the crystal structure, elemental analysis was performed on $^{t\mathrm{Bu}}$**L**Pt(C≡C-C$_6$H$_4$-*t*Bu) prior to photophysical characterization to ensure purity of the sample analyzed. Anal. Calc. for $C_{52}H_{48}N_2Pt$: C, 69.70; H, 5.40; N, 3.13 %. Found: C, 69.45; H, 5.51; N, 3.07 %.

Synthesis of 1,3-bis(4-(2-trifluoromethylphenanthridinyl))benzene platinum(IV) trichloride ^{CF3}LPtCl$_3$: A round bottom flask was charged with ^{CF3}**LH** (0.050 g, 0.088 mmol), potassium tetrachloridoplatinate (0.044 g, 0.11 mmol) and glacial acetic acid (33 mL). The mixture was heated in an oil bath set to 120 °C to reflux in open atmosphere for 3 d. The resulting suspension was cooled to room temperature and filtered to collect the deposited solid. This precipitate was washed with deionized water (~20 mL) and pentane (~20 mL), and then transferred to a round bottom flask as a chloroform suspension (50 mL). This suspension was heated to reflux in open to air for 2 d in an oil bath set to 70 °C. The mixture was then cooled to room temperature and solvent removed *in vacuo* leaving a yellow-green solid identified as a mixture of ^{CF3}**L**PtCl and ^{CF3}**L**PtCl$_3$ by integration of the ^{19}F NMR spectrum (approximately 7:93). ^{1}H NMR ($CDCl_3$, 300 MHz, 22°C): δ 10.58 (s, $^3J_{PtH}$ = 33.5 Hz, 2H; C_1-*H*), 8.91 (s, 2H; C_{13}-*H*), 8.76 (d, $^3J_{HH}$ = 8.4 Hz, 2H; C_6-*H*), 8.54 (s, 2H; C_{11}-*H*), 8.39 (d, $^3J_{HH}$ = 8.0 Hz, 2H; C_3-*H*), 8.19 (t, $^3J_{HH}$ = 8.1 Hz, 2H; C_5-*H*), 7.92 (t, $^3J_{HH}$ = 7.9 Hz, 2H; C_4-*H*), 7.75 (d, $^3J_{HH}$ = 8.2 Hz, 2H; C_{17}-*H*), 7.58 ppm (m, 1H; C_{18}-*H*). ^{19}F{^{1}H} NMR ($CDCl_3$, 282 MHz, 22 °C): δ -62.0 (93%, Pt^{IV}), -62.2 ppm (7%, Pt^{II}). HR-MS (APCI-TOF) m/z: $[M - Cl]^+$ calculated for $[C_{34}H_{17}F_6N_2PtCl_2]^+$: 833.0307; Found: 833.0251.

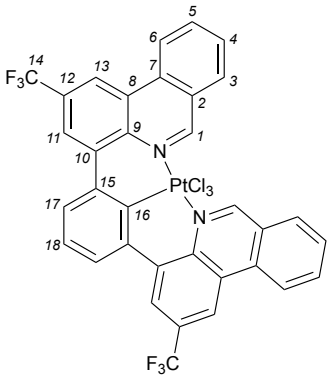

UV-Vis absorption and luminescence measurements

Absorption spectra were measured on a Biotek Instruments XS spectrometer, using quartz cuvettes of 1 cm pathlength. Steady-state luminescence spectra were measured using a Jobin Yvon FluoroMax-2 spectrofluorimeter, fitted with a red-sensitive Hamamatsu R928 photomultiplier tube; the spectra shown are corrected for the wavelength dependence of the detector, and the quoted emission maxima refer to the values after correction. Samples for emission measurements were contained within quartz cuvettes of 1 cm pathlength modified with appropriate glassware to allow connection to a high-vacuum line. Degassing was achieved via a minimum of three freeze-pump-thaw cycles whilst connected to the

vacuum manifold; final vapor pressure at 77 K was < 5×10^{-2} mbar, as monitored using a Pirani gauge. Measurements were made under this vacuum followed by corresponding aerated measurements upon allowing the solutions to equilibrate with air. Luminescence quantum yields were determined using the following equation:

$$\Phi_{sample} = (I_{sample} / I_{std}) \times (f^{abs}_{std}/f^{abs}_{sample}) \times (n_{sample}/n_{std})^2 \times \Phi_{std}$$

where I_{sample} and I_{std} are the integrated areas under the corrected emission spectra of sample and standard, f^{abs}_{sample} and f^{abs}_{std} are the respective fractions of light absorbed at the excitation wavelength employed (calculated from the corresponding absorbance A through $f^{abs} = 1–10^{–A}$), n_{sample} and n_{std} are the refractive indices of CH_2Cl_2 and H_2O respectively, and Φ_{std} is the quantum yield of the standard. The standard used was $[Ru(bpy)_3]Cl_2$ in aqueous solution, for which the now widely accepted value of Φ is 0.040±0.002.[43] The estimated uncertainty on the quantum yields obtained in this way on the instrumentation employed is up to ±20%.

Luminescence lifetimes of the complexes in air-equilibrated solutions (and also that of the acetylido complex in degassed solution, which has a short lifetime) were measured by time-correlated single-photon counting, following excitation at 405 nm with a pulsed-diode laser. The emitted light was detected at 90° using a Peltier-cooled R928 PMT after passage through a monochromator. Lifetimes for all but the acetylido complex in degassed solution, and for all complexes at 77 K, were measured following excitation with a microsecond-pulsed xenon lamp and detection using the same PMT operating in multichannel scaling mode. For all measurements, the decays were much longer than the instrument response, and data were analyzed by tail fitting to the following equation (rather than by deconvolution of the response function):

$$I(t) = I(0) \exp(–kt) + c$$

where $I(t)$ is the intensity of light detected at time t, k is the first-order rate constant for decay ($k = 1/\tau$), and c is a constant reflecting the intrinsic “dark count” during the measurement. The estimated

uncertainty in the quoted lifetimes is ±10%. Bimolecular rate constants for quenching by molecular oxygen, k_Q, were determined from the lifetimes in degassed and air-equilibrated solution, taking the concentration of oxygen in CH_2Cl_2 at 0.21 atm O_2 to be 2.2 mmol dm^{-3}.[44]

Computational Details

DFT optimizations were carried out using Gaussian16, rev. B.01[45] at the M06L/def2SVP[46–48] level of theory, using the IEFPCM[49] solvent model ($CHCl_3$) and Grimme's D3 dispersion correction with Becke-Johnson damping (D3BJ).[50] TD-DFT and single point calculations were performed at the PBE0/def2TZVP[51] level of theory using ORCA version 4.1.2,[52,53] and with the IEFPCM[49] solvent model with CH_2Cl_2. For all TD-DFT calculations the 'resolution of identity with chain-of-sphere' approximation was used with a special grid on Pt (RIJCOSX; intaccx: 4.34, 4.34, 4.67; gridx: 2,2,2; specialgridintacc: 9),[54] scalar relativistic effects using the two-component, zeroth order regular approximation (ZORA)[55] as implemented in ORCA, along with the SARC-TZVP[48] and corresponding auxiliary basis sets[55–59] on the heavy element Pt. SCF convergence and grid criteria were set to TightSCF and grid5, respectively, with the final grid criteria set to FinalGrid6. Molecular orbital analyses were carried out using the Hirshfeld partition method[60] available in Multiwfn software.[61] Avogadro[62] was employed to visualize the molecular orbitals. The results of TD-DFT were analyzed using Multiwfn[61] and spin density maps were generated using Gabedit.[63] To calculate ground-state, excited state, and reorganization energies, a previously established[20] protocol was followed. First, the S_0 geometry was optimized by restricted DFT (charge = 0 or 1, multiplicity = 1) using the crystal structure coordinates as starting input. The results were compared to the crystal structure when available to verify the accuracy of the level of theory. The T_1 geometries were then optimized with unrestricted DFT (charge = 0 or 1, multiplicity = 3) using the optimized S_0 geometry as starting input. Frequency calculations were carried out with each optimization to confirm that these structures are at a minimum. Second, the electronic energies, E_{S0} and E_{T1}, obtained from the single point calculations of S_0 and T_1 at their respective minima,

were used to estimate the adiabatic energy ($E_{adiabatic}$), where $E_{adiabatic} = E_{T1} - E_{S0}$. Next, TD-DFT was carried out on the first fifty $S_0 \rightarrow S_n$ singlet-singlet transitions with the restricted formalism (charge = 0 or 1, multiplicity = 1). Population analysis was performed to determine the relative molecular fragment contributions to the frontier MOs which contribute to the electronic transitions. Last, $E_{vert\text{-}phos}$ ($T_1 \rightarrow T_1@S_0$) was estimated as the ΔSCF between single point energies of the T_1 (charge = 0 or 1, multiplicity = 3) and $T_1@S_0$ (charge = 0 or 1, multiplicity = 1), both at the optimized T_1 geometry.

X-Ray Crystallography and Structural Data

X-ray crystal structure data was collected from multi-faceted crystals of suitable size and quality selected from a representative sample of crystals of the same habit using an optical microscope. In each case, crystals were mounted on MiTiGen loops and data collection carried out in a cold stream of nitrogen (150 K; Bruker D8 QUEST ECO; Mo Kα radiation). All diffractometer manipulations were carried out using Bruker APEX3 software.[64] Structure solution and refinement was carried out using XS, XT and XL software, embedded within the Olex2 GUI.[65] For each structure, the absence of additional symmetry was confirmed using ADDSYM incorporated in the PLATON program.[66]

Crystal structure data for **$^{t\text{Bu}}$LH** (CCDC 2095076): X-ray quality crystals were grown from a concentrated methanol solution at -15°C. Clear blocks; $C_{42}H_{44}N_2O_2$ 608.79 g/mol, monoclinic, space group *C*2/c; a = 28.8167(11) Å, b = 11.6422(4) Å, c = 21.0124(8) Å, α = 90º, β = 103.8580(10), γ = 90°, V = 6844.3(4) Å^3; Z = 8, ρ_{calcd} = 1.182 g cm^{-3}; crystal dimensions 0.1 x 0.1 x 0.1 mm; $2\theta_{max}$ = 52.96°; 80229 reflections, 7063 independent (R_{int} = 0.0841, intrinsic phasing; absorption coefficient (μ = 0.072 mm^{-1}), absorption correction semi-empirical from equivalents (SADABS); refinement (against F_o^2) with SHELXTL V6.1, 456 parameters, 0 restraints, R_1 = 0.0717 ($I > 2\sigma$) and wR_2 = 0.1739 (all data), Goof = 1.038, residual electron density 0.52/−0.45 Å^{-3}.

Crystal structure data for $^{t\mathrm{Bu}}$**L**PtCl (CCDC 2095077): X-ray quality crystals were grown from diffusion of hexanes vapor into a chloroform solution of the compound at room temperature. Yellow blocks; $C_{40}H_{35}ClN_2Pt$ 774.24 g/mol, monoclinic, space group $P2_1/c$; a = 18.6532(14) Å, b = 17.2524(14) Å, c = 9.8735(8) Å, α = 90º, β = 90.711(3), γ = 90°, V = 3177.2(4) Å^3; Z = 4, ρ_{calcd} = 1.619 g cm^{-3}; crystal dimensions 0.27 x 0.13 x 0.080 mm; $2\theta_{max}$ = 52.87°; 75037 reflections, 6506 independent (R_{int} = 0.0687, direct methods; absorption coefficient (μ = 4.532 mm^{-1}), absorption correction semi-empirical from equivalents (SADABS); refinement (against F_o^2) with SHELXTL V6.1, 404 parameters, 0 restraints, R_1 = 0.0672 ($I > 2\sigma$) and wR_2 = 0.2151 (all data), Goof = 1.117, residual electron density 2.71/−3.00 Å^{-3}.

Crystal structure data for [$^{\mathrm{CF3}}$**L**Pt(py)]PF_6 (CCDC 2095078): X-ray quality crystals were grown from diffusion of hexanes vapor into a chloroform solution of the compound at room temperature. Yellow blocks; $C_{40}H_{23}Cl_3F_{12}N_3PPt$ 1106.02 g/mol, triclinic, space group P-1; a = 9.6211(5) Å, b = 13.0472(8) Å, c = 16.7674(8) Å, α = 85.836(2)º, β = 78.008(2), γ = 68.405(2)°, V = 1914.32(18) Å^3; Z = 2, ρ_{calcd} = 1.919 g cm^{-3}; crystal dimensions 0.270 x 0.15 x 0.050 mm; $2\theta_{max}$ = 55.11°; 56169 reflections, 8819 independent (R_{int} = 0.0324, intrinsic phasing; absorption coefficient (μ = 4.011 mm^{-1}), absorption correction semi-empirical from equivalents (SADABS); refinement (against F_o^2) with SHELXTL V6.1, 541 parameters, 0 restraints, R_1 = 0.0394 ($I > 2\sigma$) and wR_2 = 0.0930 (all data), Goof = 1.079, residual electron density 2.30/−1.68 Å^{-3}.

Crystal structure data for $^{t\mathrm{Bu}}$**L**Pt(-C≡C-C_6H_6-*t*Bu)] (CCDC 2095079): X-ray quality crystals were grown from diffusion of pentane vapor into a chloroform solution of the compound at room temperature. A minor second component (5%) was identified in the crystal lattice as $^{t\mathrm{Bu}}$**L**PtCl. Yellow rods; $C_{53.44}H_{49.39}Cl_{6.05}N_2Pt$ 1129.09 g/mol, monoclinic, space group $P2_1/c$; a = 10.8107(10) Å, b = 19.1386(18) Å, c = 23.554(2) Å, α = 90º, β = 95.931(3), γ = 90°, V = 4847.3(8) Å^3; Z = 4, ρ_{calcd} = 1.547 g cm^{-3};

crystal dimensions 0.57 x 0.04 x 0.03 mm; $2\theta_{max}$ = 55.12°; 148000 reflections, 11186 independent (R_{int} = 0.0933, intrinsic phasing; absorption coefficient (μ = 3.267 mm^{-1}), absorption correction semi-empirical from equivalents (SADABS); refinement (against F_o^2) with SHELXTL V6.1, 612 parameters, 0 restraints, R_1 = 0.0507 ($I > 2\sigma$) and wR_2 = 0.1028 (all data), Goof = 1.090, residual electron density 1.62/−1.36 $Å^{-3}$.

Crystal structure data for ^{CF3}**L**$PtCl_3$ (CCDC 2095080): X-ray quality crystals were grown from diffusion of hexanes vapors into a chloroform solution of the compound at room temperature. Yellow blocks; $C_{36}H_{19}Cl_9F_6N_2Pt$ 1107.67 g/mol, monoclinic, space group *C*2/c; *a* = 15.6027(9) Å, *b* = 12.2827(6) Å, *c* = 20.3036(11) Å, α = 90º, β = 108.645(2), γ = 90°, V = 3689.0(3) $Å^3$; Z = 4, ρ_{calcd} = 1.994 g cm^{-3}; crystal dimensions 0.360 x 0.160 x 0.110 mm; $2\theta_{max}$ = 61.142°; 64502 reflections, 5661 independent (R_{int} = 0.0608, intrinsic phasing; absorption coefficient (μ = 4.519 mm^{-1}), absorption correction semi-empirical from equivalents (SADABS); refinement (against F_o^2) with SHELXTL V6.1, 246 parameters, 0 restraints, R_1 = 0.0434 ($I > 2\sigma$) and wR_2 = 0.0919 (all data), Goof = 1.075, residual electron density 1.89/−1.54 $Å^{-3}$.

ASSOCIATED CONTENT

Supporting Information. Additional X-ray figures, computational discussion, supporting figures and tables; multi-nuclear NMR and HR-MS spectra of all new compounds; crystallographic information files containing all X-ray data. CCDC 2095076-2095080 contain the supplementary crystallographic data for this paper. The data can be obtained free of charge from The Cambridge Crystallographic Data Center via www.ccdc.cam.ac.uk/structures.

The following files are available free of charge:

Supporting Information File (PDF)

Crystallographic Information Files (CIF)

AUTHOR INFORMATION

Corresponding Authors

David E. Herbert (david.herbert@umanitoba.ca)

J. A. Gareth Williams (j.a.g.williams@durham.ac.uk)

ORCIDs

Robert J. Ortiz: 0000-0001-9078-765X

Jason D. Braun: 0000-0002-5850-8048

J. A. Gareth Williams: 0000-0002-4688-3000

David E. Herbert: 0000-0001-8190-2468

Author Contributions

The manuscript was written through contributions of all authors. All authors have given approval to the final version of the manuscript.

Conflicts of Interest

There are no conflicts of interest to declare

ACKNOWLEDGMENTS

The following sources of funding are gratefully acknowledged: Natural Sciences Engineering Research Council of Canada for a Discovery Grant to DEH (RGPIN-2014-03733); the Canada Foundation for Innovation and Research Manitoba for an award in support of an X-ray diffractometer (CFI #32146); the University of Manitoba for UMGF Fellowships (RJO, JDB). I.B. Lozada is thanked for helpful discussions regarding theoretical computations.

REFERENCES

(1) Zhao, Q.; Li, F.; Huang, C. Phosphorescent Chemosensors Based on Heavy-Metal Complexes. *Chem. Soc. Rev.* **2010**, *39*, 3007–3030.

(2) Tang, W.-S.; Lu, X.-X.; Wong, K. M.-C.; Yam, V. W.-W. Synthesis, Photophysics and Binding Studies of Pt(II) Alkynyl Terpyridine Complexes with Crown Ether Pendant. Potential Luminescent Sensors for Metal Ions. *J. Mater. Chem.* **2005**, *15*, 2714–2720.

(3) Mauro, M.; Aliprandi, A.; Septiadi, D.; Kehr, N. S.; De Cola, L. When Self-Assembly Meets Biology: Luminescent Platinum Complexes for Imaging Applications. *Chem. Soc. Rev.* **2014**, *43*, 4144–4166.

(4) Baggaley, E.; Weinstein, J. A.; Williams, J. A. G. Lighting the Way to See inside the Live Cell with Luminescent Transition Metal Complexes. *Coord. Chem. Rev.* **2012**, *256*, 1762–1785.

(5) Koo, C.-K.; Wong, K.-L.; Man, C. W.-Y.; Lam, Y.-W.; So, L. K.-Y.; Tam, H.-L.; Tsao, S.-W.; Cheah, K.-W.; Lau, K.-C.; Yang, Y.-Y.; Chen, J.-C.; Lam, M. H.-W. A Bioaccumulative Cyclometalated Platinum(II) Complex with Two-Photon-Induced Emission for Live Cell Imaging. *Inorg. Chem.* **2009**, *48*, 872–878.

(6) Kalinowski, J.; Fattori, V.; Cocchi, M.; Williams, J. A. G. Light-Emitting Devices Based on Organometallic Platinum Complexes as Emitters. *Coord. Chem. Rev.* **2011**, *255*, 2401–2425.

(7) Wong, W.-Y.; Ho, C.-L. Heavy Metal Organometallic Electrophosphors Derived from Multi-Component Chromophores. *Coord. Chem. Rev.* **2009**, *253*, 1709–1758.

(8) Xiang, H.-F.; Lai, S.-W.; Lai, P. T.; Che, C.-M. Phosphorescent Platinum(II) Materials for OLED Applications. In *Highly Efficient OLEDs with Phosphorescent Materials*; Yersin, H., Ed.; Wiley-VCH: Weinheim, Germany, 2007; pp 259–282.

(9) Chakraborty, S.; Wadas, T. J.; Hester, H.; Schmehl, R.; Eisenberg, R. Platinum Chromophore-Based Systems for Photoinduced Charge Separation: A Molecular Design Approach for Artificial Photosynthesis. *Inorg. Chem.* **2005**, *44*, 6865–6878.

(10) Gourlaouen, C.; Daniel, C. Spin–Orbit Effects in Square-Planar Pt(II) Complexes with Bidentate and Terdentate Ligands: Theoretical Absorption/Emission Spectroscopy. *Dalton Trans.* **2014**, *43*, 17806–17819.

(11) Li, K.; Tong, G. S. M.; Wan, Q.; Cheng, G.; Tong, W.-Y.; Ang, W.-H.; Kwong, W.-L.; Che, C.-M. Highly Phosphorescent Platinum(II) Emitters: Photophysics, Materials and Biological Applications. *Chem. Sci.* **2016**, *7*, 1653–1673.

(12) Crites, D. K.; Cunningham, C. T.; McMillin, D. R. Remarkable Substituent Effects on the Photophysics of Pt(4′-X-trpy)Cl^+ Systems (Trpy = 2,2′; 6′,2″-Terpyridine). *Inorg. Chim. Acta* **1998**, *273*, 346–353.

(13) Williams, J. A. G.; Beeby, A.; Davies, E. S.; Weinstein, J. A.; Wilson, C. An Alternative Route to Highly Luminescent Platinum(II) Complexes: Cyclometalation with N^C^N-Coordinating Dipyridylbenzene Ligands. *Inorg. Chem.* **2003**, *42*, 8609–8611.

(14) Garner, K. L.; Parkes, L. F.; Piper, J. D.; Williams, J. A. G. Luminescent Platinum Complexes with Terdentate Ligands Forming 6-Membered Chelate Rings: Advantageous and Deleterious Effects in N^N^N and N^C^N-Coordinated Complexes. *Inorg. Chem.* **2010**, *49*, 476–487.

(15) Bailey, J. A.; Hill, M. G.; Marsh, R. E.; Miskowski, V. M.; Schaefer, W. P.; Gray, H. B. Electronic Spectroscopy of Chloro(Terpyridine)Platinum(II). *Inorg. Chem.* **1995**, *34*, 4591–4599.

(16) Abrahamsson, M.; Jäger, M.; Österman, T.; Eriksson, L.; Persson, P.; Becker, H.-C.; Johansson, O.; Hammarström, L. A 3.0 ms Room Temperature Excited State Lifetime of a Bistridentate Ru^{II} −Polypyridine Complex for Rod-like Molecular Arrays. *J. Am. Chem. Soc.* **2006**, *128*, 12616–12617.

(17) Brown, D. G.; Sanguantrakun, N.; Schulze, B.; Schubert, U. S.; Berlinguette, C. P. Bis(Tridentate) Ruthenium-Terpyridine Complexes Featuring Microsecond Excited-State Lifetimes. *J. Am. Chem. Soc.* **2012**, *134*, 12354–12357.
(18) Wood, E. A.; Gildea, L. F.; Yufit, D. S.; Williams, J. A. G. Synthesis, Structures and Luminescence Properties of N^C^N-Coordinated Platinum(II) Complexes Based on an Anthracene Core: A Red Shift and a Twist. *Polyhedron* **2021**, *207*, 115401.
(19) Mandapati, P.; Braun, J. D.; Killeen, C.; Davis, R. L.; Williams, J. A. G.; Herbert, D. E. Luminescent Platinum(II) Complexes of N^N-^N Amido Ligands with Benzannulated N-Heterocyclic Donor Arms: Quinolines Offer Unexpectedly Deeper Red Phosphorescence than Phenanthridines. *Inorg. Chem.* **2019**, *58*, 14808–14817.
(20) Mandapati, P.; Braun, J. D.; Lozada, I. B.; Williams, J. A. G.; Herbert, D. E. Deep-Red Luminescence from Platinum(II) Complexes of N^N−^N-Amido Ligands with Benzannulated N-Heterocyclic Donor Arms. *Inorg. Chem.* **2020**, *59*, 12504–12517.
(21) Lersch, M.; Tilset, M. Mechanistic Aspects of C−H Activation by Pt Complexes. *Chem. Rev.* **2005**, *105*, 2471–2526.
(22) Mandapati, P.; Giesbrecht, P. K.; Davis, R. L.; Herbert, D. E. Phenanthridine-Containing Pincer-like Amido Complexes of Nickel, Palladium, and Platinum. *Inorg. Chem.* **2017**, *56*, 3674–3685.
(23) Lozada, I. B.; Huang, B.; Stilgenbauer, M.; Beach, T.; Qiu, Z.; Zheng, Y.; Herbert, D. E. Monofunctional Platinum(II) Anticancer Complexes Based on Multidentate Phenanthridine-Containing Ligand Frameworks. *Dalton Trans.* **2020**, *49*, 6557–6560.
(24) Period covered shutdown of all non-essential activities during the initial months of the COVID-19 pandemic of 2020.
(25) Juliá, F.; Bautista, D.; Fernández-Hernández, J. M.; González-Herrero, P. Homoleptic Tris-Cyclometalated Platinum(IV) Complexes: A New Class of Long-Lived, Highly Efficient ^{3}LC Emitters. *Chem. Sci.* **2014**, *5*, 1875–1880.
(26) Newkome, G. R.; Theriot, K. J.; Fronczek, F. R.; Villar, B. Synthesis and Characterization of Metalated and Cyclometalated Platinum(II) and Platinum(IV) Complexes of .Beta.-Diesters. *Organometallics* **1989**, *8*, 2513–2523.
(27) Mondal, R.; Giesbrecht, P. K.; Herbert, D. E. Nickel(II), Copper(I) and Zinc(II) Complexes Supported by a (4-Diphenylphosphino)Phenanthridine Ligand. *Polyhedron* **2016**, *108*, 156–162.
(28) Crosby, S. H.; Clarkson, G. J.; Deeth, R. J.; Rourke, J. P. Platinum(IV) DMSO Complexes: Synthesis, Isomerization, and Agostic Intermediates. *Organometallics* **2010**, *29*, 1966–1976.
(29) Giménez, N.; Lalinde, E.; Lara, R.; Moreno, M. T. Design of Luminescent, Heteroleptic, Cyclometalated PtII and PtIV Complexes: Photophysics and Effects of the Cyclometalated Ligands. *Chem. Eur. J.* **2019**, *25*, 5514–5526.
(30) Ionescu, A.; Godbert, N.; Aiello, I.; Ricciardi, L.; Deda, M. L.; Crispini, A.; Sicilia, E.; Ghedini, M. Anionic Cyclometalated Pt(II) and Pt(IV) Complexes Respectively Bearing One or Two 1,2-Benzenedithiolate Ligands. *Dalton Trans.* **2018**, *47*, 11645–11657.
(31) Cárdenas, D. J.; Echavarren, A. M.; Ramírez de Arellano, M. C. Divergent Behavior of Palladium(II) and Platinum(II) in the Metalation of 1,3-Di(2-pyridyl)benzene. *Organometallics* **1999**, *18*, 3337–3341.
(32) Yang, L.; Powell, D. R.; Houser, R. P. Structural Variation in Copper(i) Complexes with Pyridylmethylamide Ligands: Structural Analysis with a New Four-Coordinate Geometry Index, T4. *Dalton Trans.* **2007**, 955–964.
(33) Rochester, D. L.; Develay, S.; Záliš, S.; Williams, J. A. G. Localised to Intraligand Charge-Transfer States in Cyclometalated Platinum Complexes: An Experimental and Theoretical Study into the Influence of Electron-Rich Pendants and Modulation of Excited States by Ion Binding. *Dalton Trans.* **2009**, 1728–1741.

(34) Braun, J. D.; Lozada, I. B.; Kolodziej, C.; Burda, C.; Newman, K. M. E.; van Lierop, J.; Davis, R. L.; Herbert, D. E. Iron(II) Coordination Complexes with Panchromatic Absorption and Nanosecond Charge-Transfer Excited State Lifetimes. *Nat. Chem.* **2019**, *11*, 1144–1150.
(35) Bossi, A.; Rausch, A. F.; Leitl, M. J.; Czerwieniec, R.; Whited, M. T.; Djurovich, P. I.; Yersin, H.; Thompson, M. E. Photophysical Properties of Cyclometalated Pt(II) Complexes: Counterintuitive Blue Shift in Emission with an Expanded Ligand π System. *Inorg. Chem.* **2013**, *52*, 12403–12415.
(36) Mondal, R.; Lozada, I. B.; Davis, R. L.; Williams, J. A. G.; Herbert, D. E. Site-Selective Benzannulation of *N*-Heterocycles in Bidentate Ligands Leads to Blue-Shifted Emission from $[(P\text{^}N)Cu]_2(\mu\text{-}X)_2$ Dimers. *Inorg. Chem.* **2018**, *57*, 4966–4978.
(37) Flamigni, L.; Barbieri, A.; Sabatini, C.; Ventura, B.; Barigelletti, F. Photochemistry and Photophysics of Coordination Compounds: Iridium. In *Photochemistry and Photophysics of Coordination Compounds II*; Balzani, V., Campagna, S., Eds.; Springer Berlin Heidelberg: Berlin, Heidelberg, 2007; pp 143–203. https://doi.org/10.1007/128_2007_131.
(38) Mondal, R.; Lozada, I. B.; Davis, R. L.; Williams, J. A. G.; Herbert, D. E. Exploiting Synergy between Ligand Design and Counterion Interactions to Boost Room Temperature Phosphorescence from Cu(I) Compounds. *J. Mater. Chem. C* **2019**, *7*, 3772–3778.
(39) Brulatti, P.; Gildea, R. J.; Howard, J. A. K.; Fattori, V.; Cocchi, M.; Williams, J. A. G. Luminescent Iridium(III) Complexes with NCN-Coordinated Terdentate Ligands: Dual Tuning of the Emission Energy and Application to Organic Light-Emitting Devices. *Inorg. Chem.* **2012**, *51*, 3813–3826.
(40) Uoyama, H.; Goushi, K.; Shizu, K.; Nomura, H.; Adachi, C. Highly Efficient Organic Light-Emitting Diodes From Delayed Fluorescence. *Nature* **2012**, *492*, 234–238.
(41) Mydlak, M.; Mauro, M.; Polo, F.; Felicetti, M.; Leonhardt, J.; Diener, G.; De Cola, L.; Strassert, C. A. Controlling Aggregation in Highly Emissive Pt(II) Complexes Bearing Tridentate Dianionic N-N-N Ligands. Synthesis, Photophysics, and Electroluminescence. *Chem. Mater.* **2011**, *23*, 3659–3667.
(42) Haque, A.; Xu, L.; Al-Balushi, R. A.; Al-Suti, M. K.; Ilmi, R.; Guo, Z.; Khan, M. S.; Wong, W.-Y.; Raithby, P. R. Cyclometallated Tridentate Platinum(II) Arylacetylide Complexes: Old Wine in New Bottles. *Chem. Soc. Rev.* **2019**, *48*, 5547–5563.
(43) Suzuki, K.; Kobayashi, A.; Kaneko, S.; Takehira, K.; Yoshihara, T.; Ishida, H.; Shiina, Y.; Oishi, S.; Tobita, S. Reevaluation of Absolute Luminescence Quantum Yields of Standard Solutions Using a Spectrometer with an Integrating Sphere and a Back-Thinned CCD Detector. *Phys. Chem. Chem. Phys.* **2009**, *11*, 9850–9860.
(44) Murov, S. L.; Carmichael, I.; Hug, G. L. *Handbook of Photochemistry, 2nd Ed.*; Marcel Dekker: New York, 1993.
(45) Frisch, M. J.; Trucks, G. W.; Schlegel, H. B.; Scuseria, G. E.; Robb, M. A.; Cheeseman, J. R.; Scalmani, G.; Barone, V.; Petersson, G. A.; Nakatsuji, H.; Li, X.; Caricato, M.; Marenich, A. V.; Bloino, J.; Janesko, B. G.; Gomperts, R.; Mennucci, B.; Hratchian, H. P.; Ortiz, J. V.; Izmaylov, A. F.; Sonnenberg, J. L.; Williams-Young, D.; Ding, F.; Lipparini, F.; Egidi, F.; Goings, J.; Peng, B.; Petrone, A.; Henderson, T.; Ranasinghe, D.; Zakrzewski, V. G.; Gao, J.; Rega, N.; Zheng, G.; Liang, W.; Hada, M.; Ehara, M.; Toyota, K.; Fukuda, R.; Hasegawa, J.; Ishida, M.; Nakajima, T.; Honda, Y.; Kitao, O.; Nakai, H.; Vreven, T.; Throssell, K.; Montgomery, J. A.; Peralta, J. E.; Ogliaro, F.; Bearpark, M. J.; Heyd, J. J.; Brothers, E. N.; Kudin, K. N.; Staroverov, V. N.; Keith, T. A.; Kobayashi, R.; Normand, J.; Raghavachari, K.; Rendell, A. P.; Burant, J. C.; Iyengar, S. S.; Tomasi, J.; Cossi, M.; Millam, J. M.; Klene, M.; Adamo, C.; Cammi, R.; Ochterski, J. W.; Martin, R. L.; Morokuma, K.; Farkas, O.; Foresman, J. B.; Fox, D. J. *Gaussian 16, Revision B.01*; Gaussian 16, Revision B.01, Gaussian, Inc., Wallingford CT; Gaussian, Inc.: Wallingford CT, 2016.

(46) Zhao, Y.; Truhlar, D. G. A New Local Density Functional for Main-Group Thermochemistry, Transition Metal Bonding, Thermochemical Kinetics, and Noncovalent Interactions. *J. Chem. Phys.* **2006**, *125*, 194101.
(47) Andrae, D.; Häußermann, U.; Dolg, M.; Stoll, H.; Preuß, H. Energy-Adjustedab Initio Pseudopotentials for the Second and Third Row Transition Elements. *Theoret. Chim. Acta* **1990**, *77*, 123–141.
(48) Weigend, F.; Ahlrichs, R. Balanced Basis Sets of Split Valence, Triple Zeta Valence and Quadruple Zeta Valence Quality for H to Rn: Design and Assessment of Accuracy. *Phys. Chem. Chem. Phys.* **2005**, *7*, 3297–3305.
(49) Marenich, A. V.; Cramer, C. J.; Truhlar, D. G. Universal Solvation Model Based on Solute Electron Density and on a Continuum Model of the Solvent Defined by the Bulk Dielectric Constant and Atomic Surface Tensions. *J. Phys. Chem. B* **2009**, *113*, 6378–6396.
(50) Grimme, S.; Ehrlich, S.; Goerigk, L. Effect of the Damping Function in Dispersion Corrected Density Functional Theory. *J. Comput. Chem.* **2011**, *32*, 1456–1465.
(51) Adamo, C.; Barone, V. Toward Reliable Density Functional Methods without Adjustable Parameters: The PBE0 Model. *J. Chem. Phys.* **1999**, *110*, 6158–6170.
(52) Neese, F. The ORCA Program System. *WIREs Comput. Mol. Sci.* **2012**, *2* (1), 73–78.
(53) Neese, F. Software Update: The ORCA Program System, Version 4.0. *WIREs Comput. Mol. Sci.* **2018**, *8*, e1327.
(54) Neese, F.; Wennmohs, F.; Hansen, A.; Becker, U. Efficient, Approximate and Parallel Hartree–Fock and Hybrid DFT Calculations. A 'Chain-of-Spheres' Algorithm for the Hartree–Fock Exchange. *Chem. Phys.* **2009**, *356*, 98–109. https://doi.org/10.1016/j.chemphys.2008.10.036.
(55) Weigend, F. Accurate Coulomb-Fitting Basis Sets for H to Rn. *Phys. Chem. Chem. Phys.* **2006**, *8*, 1057–1065.
(56) Pantazis, D. A.; Neese, F. All-Electron Scalar Relativistic Basis Sets for the Lanthanides. *J. Chem. Theory Comput.* **2009**, *5*, 2229–2238.
(57) Pantazis, D. A.; Chen, X.-Y.; Landis, C. R.; Neese, F. All-Electron Scalar Relativistic Basis Sets for Third-Row Transition Metal Atoms. *J. Chem. Theory Comput.* **2008**, *4*, 908–919.
(58) Pantazis, D. A.; Neese, F. All-Electron Scalar Relativistic Basis Sets for the 6p Elements. *Theor Chem Acc* **2012**, *131*, 1292–1298.
(59) Pantazis, D. A.; Neese, F. All-Electron Scalar Relativistic Basis Sets for the Actinides. *J. Chem. Theory Comput.* **2011**, *7*, 677–684.
(60) Hirshfeld, F. L. Bonded-Atom Fragments for Describing Molecular Charge Densities. *Theoret. Chim. Acta* **1977**, *44*, 129–138.
(61) Lu, T.; Chen, F. Multiwfn: A Multifunctional Wavefunction Analyzer. *J. Comput. Chem.* **2012**, *33*, 580–592.
(62) Hanwell, M. D.; Curtis, D. E.; Lonie, D. C.; Vandermeersch, T.; Zurek, E.; Hutchison, G. R. Avogadro: An Advanced Semantic Chemical Editor, Visualization, and Analysis Platform. *J Cheminform* **2012**, *4*, 17.
(63) Allouche, A.-R. Gabedit—A Graphical User Interface for Computational Chemistry Softwares. *Journal of Computational Chemistry* **2011**, *32* (1), 174–182.
(64) Bruker-AXS. *APEX3 V2016.1-0*; Madison, Wisconsin, USA, 2016.
(65) Dolomanov, O. V.; Bourhis, L. J.; Gildea, R. J.; Howard, J. A. K.; Puschmann, H. OLEX2: A Complete Structure Solution, Refinement and Analysis Program. *J. Appl. Crystallogr.* **2009**, *42*, 339–341.
(66) Spek, A. L. Structure Validation in Chemical Crystallography. *Acta Cryst.* **2009**, *D65*, 148–155.

For Table of Contents Only

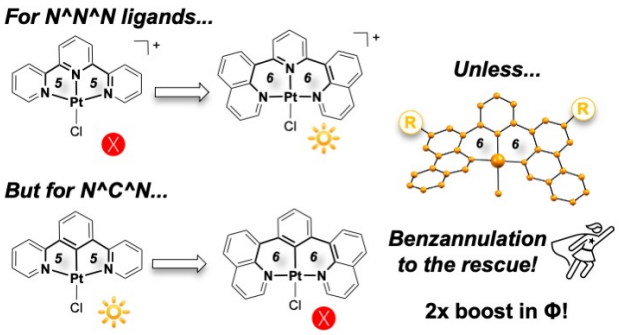

A series of brightly emissive platinum(II) complexes is presented, each supported by cyclometallated *N^C⁻^N*-coordinating ligands derived from 1,3-di(4-phenathridinyl)benzene which form two, 6-membered chelate rings. The boost in photophysical properties such as the quantum yield indicates that site-selective benzannulation of the quinolinyl side-arms can offset the previously described deleterious effect of changing the chelate ring-size from 5 atoms to 6 in *N^C^N*-coordinated Pt(II) phosphors.